Terr. Atmos. Ocean. Sci., Vol. 32, No. 6, Part III, 1227-1253, December 2021 doi: 10.3319/TAO.2021.12.26.01

Water of eastern Taiwan mud volcanoes. Part I. H, triple O, triple Sr isotopes, and trace elements of Lo-Shan mud volcano

Hung-Chun Chao[1, 2, *], Chen-Feng You[3, 4], In-Tian Lin[5], Hsueh-Yu Lu[1, 2], Hou-Chun Liu[3], and Chuan-Hsiung Chung[3, 4]

[1] *Department of Earth and Environmental Sciences, National Chung Cheng University, Chiayi County, Taiwan*
[2] *Environment and Disaster Monitoring Center, National Chung Cheng University, Chiayi County, Taiwan*
[3] *Department of Earth Sciences, National Cheng Kung University, Tainan City, Taiwan*
[4] *Earth Dynamic System Research Center, National Cheng Kung University, Tainan City, Taiwan*
[5] *Exploration & Development Research Institute, CPC Corporation, Taiwan*

Article history:
Received 17 October 2021
Revised 16 December 2021
Accepted 26 December 2021

Keywords:
Mud volcano, Radiogenic Sr isotope, Stable Sr isotope, Sediment-hosted geothermal system, Water-rock interaction, Triple oxygen isotopes

Citation:
Chao, H.-C., C.-F. You, I.-T. Lin, H.-Y. Lu, H.-C. Liu, and C.-H. Chung, 2021: Water of eastern Taiwan mud volcanoes. Part I. H, triple O, triple Sr isotopes, and trace elements of Lo-Shan mud volcano. Terr. Atmos. Ocean. Sci., 32, 1227-1253, doi: 10.3319/TAO.2021.12.26.01

ABSTRACT

Mud volcano (MV) is one of the most important passageways for deep seated volatile materials to migrate back to Earth's surface in sedimentary basins and subduction zones. Waters of MV fluid emitted from 18 mud pools in MV Luo-Shan (LS) in eastern Taiwan were sampled from the year 2002 to the year 2021. Major and trace components as well as H, triple O ($\delta^{18}O$ and $\Delta^{17}O$) and triple Sr isotopes ($^{87}Sr/^{86}Sr$ and $\delta^{88}Sr$) were measured. The results show that major components of water are Cl^-, Na, and Ca. Compared with seawater, water of MV LS reveals similar chemical characteristics with low-temperature ridge-flank hydrothermal spring and marine pore water in reducing condition. Limited spatial and temporal variation of major components as well as H, triple O and $^{87}Sr/^{86}Sr$ indicates waters emitted by mud pools come from the same source regionally. Slightly radiogenic $^{87}Sr/^{86}Sr$ at southern mud pools and before the year 2003 denotes different fluid reservoir from northern ones. Small $^{87}Sr/^{86}Sr$ variation in waters of northern mud pools indicates near surface mixing from 2 fluid reservoirs. The correlation among all components reveals sediment component addition is the major factor and evaporation is the key factor for conservative elements. In summary, waters expelled by MV LS mud pools originate from the same regional source, and their trace element composition such as Mg, K, Sr as well as $^{87}Sr/^{86}Sr$ slightly varies, depending on the location of the reservoir they are hosted. A stable source with small vibration of fluid reservoir of MV LS is indicated during the 19-years investigation period.

1. INTRODUCTION

Mud volcano is one of the most effective passages for the fluids at depth to migrate through thick sediments to the surface. It is a diapiric structure resulting from tectonic compaction and hydrocarbon gas weakening in convergent margins where soft, thick, and fine-grained mud is rapidly deposited. Development of the mud diapir or the fault provides the pathway for the fluid to migrate upward and forms the shape of MV on the Earth's surface (Milkov 2000; Dimitrov 2002; Kopf 2002; Mazzini and Etiope 2017). The terrestrial MVs are distributed on tectonically convergent region such as Italy, Azerbaijan, Romania, Taman (Russia), Georgia, Iran, Pakistan, Andaman (India), Indonesia, Taiwan, Japan, Sakhalin (Russia), Trinidad and so on (Dia et al. 1999; Delisle et al. 2002; Etiope et al. 2002, 2011a, b; Planke et al. 2003; Shakirov et al. 2004; Yang et al. 2004; You et al. 2004; Lavrushin et al. 2005, 2015; Mazzini et al. 2007, 2009; Deville and Guerlais 2009; Ray et al. 2013; Farhadian Babadi et al. 2019), and there are probably 10 times more marine MVs than terrestrial ones (Milkov 2000; Mazzini and Etiope 2017).

The mediums emitted by MVs come in three phases: gas, water, and solid. The gases are mainly methane (> 90%) with minor amounts of nitrogen, argon, carbon dioxide, ethane, and higher hydrocarbon gases (Etiope et al.

* *Corresponding author*
E-mail: hcchao@ccu.edu.tw

2002, 2007, 2009; Shakirov et al. 2004; Yang et al. 2004; Chao et al. 2010; Sun et al. 2010). Some MV gases are dominated by CO_2 (Etiope et al. 2002; Shakirov et al. 2004; Yang et al. 2004: Chao et al. 2010). These atypical MVs are probably associated with the sediment-hosted geothermal system (Procesi et al. 2019). More than 76% of MVs expel thermogenic methane and only 4% expel microbial methane. The rest of the MVs expel mixed gases (Etiope et al. 2009). Generally speaking, the water expelled by MVs originates from marine sedimentary pore fluids. It may have experienced important diagenesis and/or have been influenced by clay dehydration and water-rock interaction. Additionally, it may pass through halide dissolution and may mix with groundwater, surface runoff, and meteoric water near land surface (Bray and Karig 1985; Dia et al. 1999; Dahlmann and de Lange 2003; You et al. 2004; Mazzini et al. 2009). The solid matter is mainly derived from the ambient sediments surrounding the fluid reservoirs or the migration channel. They are mostly clay minerals, such as smectite, illite, kaolinite and chlorite as well as other minerals like quartz and calcite (Shih 1967; Dia et al. 1999; Kopf and Deyhle 2002; Farhadian Babadi et al. 2019). The origination of all three phases can be decoupled from each other (Sun et al. 2010; Mazzini et al. 2018).

Waters discharged by eastern Taiwan MVs have different chemical characteristics from those expelled by western ones. The evidence of major elements as well as $^{87}Sr/^{86}Sr$ show signature of rock-rock interaction with igneous rocks (You et al. 2004; Chao et al. 2013). The geological sedimentary structure emits waters containing geothermal signal. This hybrid characteristic matches the sediment-hosted geothermal system (Procesi et al. 2019). Although large $^{87}Sr/^{86}Sr$ variation in different mud pools are reported in nearby MV Lei-Gong-Huo (LGH; Chao et al. 2013, 2022), Sr isotopes of the water in MV Luo-Shan show consistent igneous characteristics for all mud pools collected in this area (You et al. 2004; Chao et al. 2013), implying different source condition between the 2 MVs.

In this study, water samples from 18 mud pools at MV LS were collected from the year 2002 to the year 2021. The major as well as trace ions/elements, hydrogen, triple oxygen, and triple strontium isotopic compositions were measured. The systematic measurements with 19-year investigations will help to understand the source of the fluid, underground fluid reservoirs as well as chemical and isotopic variation of MV LS.

2. METHODOLOGY

2.1 Geological Background and Site Description

The Taiwan mountain belt formed as a result of arc-continent collision between the Philippine Sea Plate and the Eurasian Plate and one of the possible suture zones is the Longitudinal Valley, situated between the Central Range and the Coastal Range (Li 1976; Teng 1990). The Luzon Arc moves northeast toward the Asian continent at an average rate of 7 cm per year (Yu et al. 1997). Across the Longitudinal Valley Fault (LVF), the movement decreases dramatically to 2 cm per year (Ching et al. 2011). The highly deformed Lichi Mélange formation, which was the forearc basin and composed of chaotic mudstone mixed with fragments of oceanic crust (Chang et al. 2000), may be the substance that absorbs the movement (Ching et al. 2011) and provides the suitable environment for the formation of MVs.

There are 3 MVs located along the Longitudinal Valley in eastern Taiwan (Fig. 1a), which are Luo-Shan (previously also named Yencheng by Shih 1967), Shih-Men-Wai, and Lei-Gong-Huo from north to south (Shih 1967). All the MVs are located on Lichi Mélange as well as the hanging wall of Lichi Fault and the foothill of the Coastal Range (Fig. 1b). This area happens to be extensional co-seismically (Ching et al. 2007; Lin et al. 2010) and the channels of MV fluids are in unclamping conditions (Bonini et al. 2016; Bonini 2021), enhancing the eruption activities (Jiang et al. 2011).

MV LS is the northernmost MV in eastern Taiwan. Dozens of swamp-like mud pools are distributed linearly in the area approximately 1 km in length and 200 m in width with the orientation of N20°E (NNE-SSW), parallel to the strike of the major faults. Based on the location of the mud pools, six groups, A to F, are classified from north to south (Fig. 1c). Group A has one long-lasting mud pool, LS-A1, while others are short-lived ones. Mud pools in group B all exist temporally. Group C is in a private yard, and thus not sampled in this study. Another long-lived mud pool is in group D, LS-D1. LS-E1 has existed since the 2008 investigation, and the path to group F was broken after 2015, as a result, only the samples collected before 2008 are discussed in this study.

MV LS emits predominantly methane (> 90%), similar to MVs in western Taiwan. However, low CO_2 content (< 0.2%) and higher N_2 concentration (> 5%) with mantle helium signals (Yang et al. 2003, 2004; Chao et al. 2010) show different gas compositions. MV LS emits thermogenic methane (Chao et al. 2010; Sun et al. 2010) and the formation temperature of LS-A1 estimated by the chemical composition falls within 67 to 97°C, indicating that the origination depth of waters are similar to or shallower than the gases (Chao et al. 2011, 2022).

2.2 Sampling

MV samples have been collected since October 2002. More intense sampling were performed from October 2015 to July 2016 monthly and from January 2017 to 2021 yearly. The fluid samples were collected right below the gas bubbling area using four 50 cm^3 pre-weighted polypropylene (PP) centrifuge tubes. The temperature, pH, and oxidation-reduction potential (ORP) values were obtained on site with

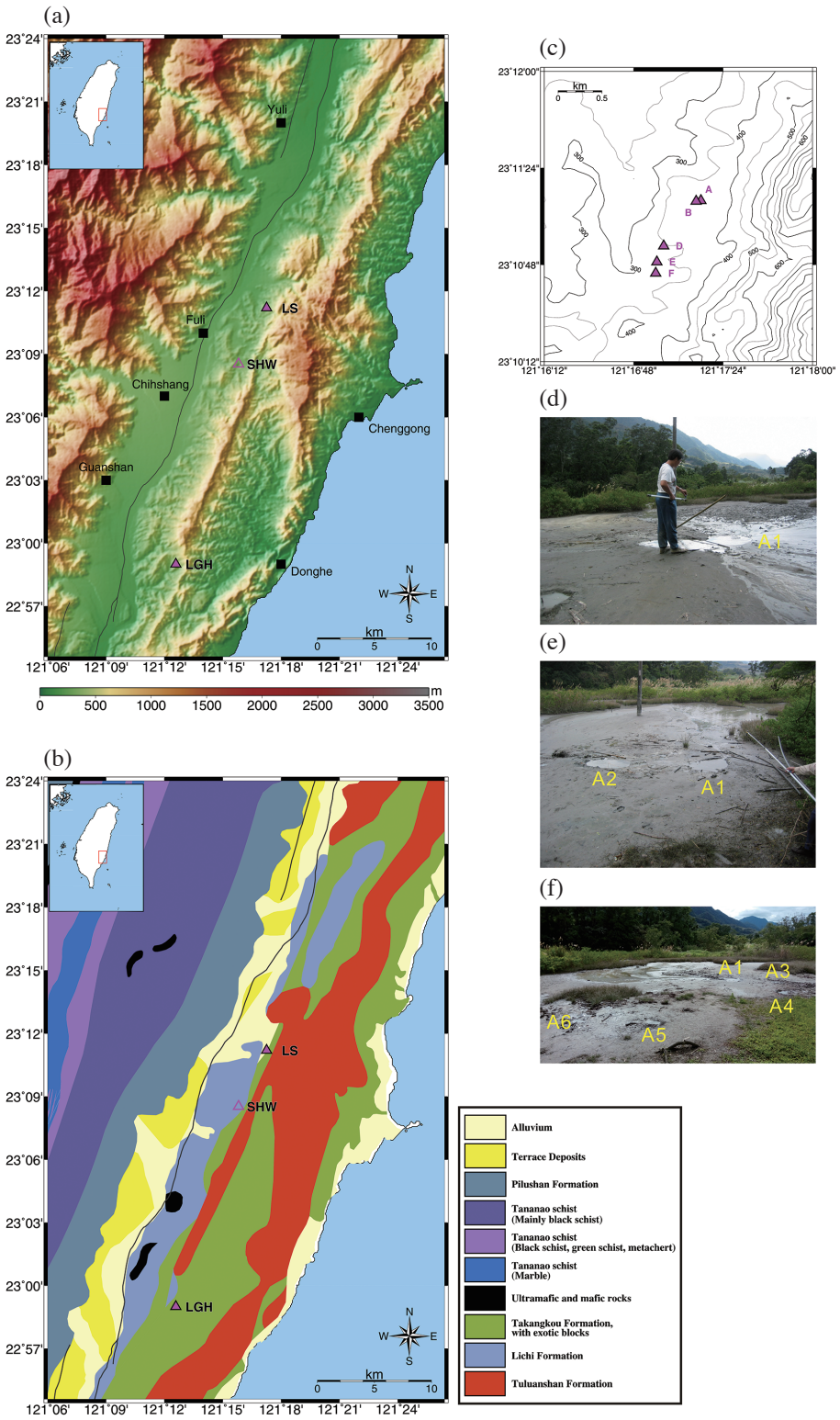

Fig. 1. (a) MVs in eastern Taiwan (triangles), open symbol denotes vanished MV, solid line indicates major fault. (b) Geologic map adopted from Central Geologic Survey, MOEA, Taiwan (https://www.moeacgs.gov.tw), solid line indicates major fault. (c) Linear distribution of 5 groups at MV LS. (d) Photograph of LS-A1_2002 taken on 2002-11-24. (e) Photograph of LS-A1 and LS-A2 on 2008-12-14. (f) Spatial distribution of satellite mud pools at group A. Photograph was taken on 2017-01-16.

a WalkLAB® TI9000 temperature compensation pH meter. Flux of expelling gas is measured by inverting a volumetric PP beaker in the bubbling area and slurry flux is measured by a volumetric PP beaker under the slurry overflowing incision The time to fill the beaker was determined by a stopwatch. The average flux was achieved through 7 measurements on site. Field samples were shipped back to the laboratory at low temperature. The samples were filtered with 0.45 μm nylon membrane filters after being centrifuged by 2560 ×g relative centrifugal force (RCF) for 30 minutes. The residual solids were dried in the oven at 50°C overnight. The weight of dried mud along with the centrifuge tube was measured and the percentage of mud weight was obtained by the dry weight over raw weight after the weight of the centrifuge tube was deducted. Half of the filtered solutions were acidified with purified concentrated nitric acid to pH < 2 for the determination of major and trace elements, and Sr isotopes. Unacidified samples were preserved for the measurement of anion concentrations, total alkalinity, and H and triple O isotopes. All samples were kept at 4°C in the refrigerator for later analysis.

2.3 Chemical Composition in the Fluids

Dissolved anions (Cl^-) were determined using ion chromatography (Dionex® ICS-3000) with the precision better than 5%. Quality assurance was obtained via diluted international seawater standard IAPSO. Chloride concentration of diluted IAPSO was calculated based on the salinity and the equation established by Millero et al. (2008). Major and some trace elements (B, Ba, Ca, Fe, K, Li, Mg, Mn, Na, S, Si, and Sr) were measured using Agilent 5100 inductively coupled plasma optical emission spectrometry (ICP-OES) with a precision of better than 3%. Other trace elements (Al, As, Br, Co, Cs, Cu, Ge, I, Mo, Ni, Pb, Rb, Sb, Ti, U, and Zn) were measured with Agilent 7500cx quadrupole inductively coupled plasma mass spectrometer (ICP-Q-MS). Samples before 2008 only had trace elements Br, I, Rb, U measured with high resolution inductively coupled plasma mass spectrometer (HR-ICP-MS, Element II, Thermo Fisher Scientific). Chemical composition of the year 2008 samples were published (Chao et al. 2011) but analyzed again in this study. The double check findings show comparable results except K concentration. New results show better accuracy which is confirmed by ICP-Q-MS. Therefore, new K concentration of the year 2008 samples is updated to Table 1. Due to high Cl, Na, Ca in the samples, matrix-matched calibration standards were prepared, and the quality assurance was obtained through 3 reference materials, SLRS-5, CASS-4, and NASS-5. The results fall in the range of 20% certified values except As, Co, and Ni. Arsenic is seriously overprinted by isobar $^{35}Cl^{40}Ar^+$ while ^{59}Co and ^{60}Ni have isobaric interferences by calcium oxide. Since the intensity of the signals was too low to be quantified in collision mode, numerical normalization is applied. The 43/59 and 43/60 ratios of samples spiking with concentration matching Cl and Ca were monitored before and after each 10 samples run. The intensity and ratios were applied to remove the potion from the interferences. The intensity of m/z 75 was deduced by intensity of m/z 77 and multiplying by $^{35}Cl/^{37}Cl$ ratio to correct the contribution from $^{35}Cl^{40}Ar^+$. Before Cl correction, the intensity of m/z 77 contributed by Se was removed by monitoring m/z 82. After numerical normalization, the results of reference materials fall in 20% range of certified values for the three elements.

Total alkalinity (TA) was measured by the acid titration (Metrohm® 905 Titrando) with the precision better than 1%, estimated by repeating analyses of the sample (n = 3) and in-house prepared bicarbonate standard.

2.4 Hydrogen and Triple Oxygen Isotopes

H and triple O isotopes were obtained by the cavity ring-down spectroscopy (CRDS, H_2O isotope analyzer, Picarro L2140-i) installed in Exploration & Development Research Institute, CPC Corporation, Taiwan (EDRI). Instrumental fractionation was corrected by measuring two international standards (V-SMOW2 and SLAP2). This correction was certified by a third international standard (GISP). For drift correction and quality control, 4 USGS standards of known δD and $\delta^{18}O$ values (USGS-45; USGS-47; USGS-48; USGS-50) were analyzed after six consecutive samples run. The reproducibility of δD, $\delta^{18}O$, and $\delta^{17}O$ is better than 0.1, 0.03, and 0.02‰ (2σ, n = 6) respectively, by repeating analyses of selected samples. All δD and $\delta^{18}O$ isotopic results reported in this study were normalized to V-SMOW2. Mass independent $\Delta^{17}O$ results were calculated following Sharp et al. (2018):

$$\Delta^{17}O = \delta^{17}O - \lambda\delta^{18}O + \gamma \ (‰) \quad (1)$$

where $\lambda = 0.528$ and γ is generally assumed to be 0.

2.5 Triple Sr Isotopes

The separation and purification of Sr were performed using an extraction chromatography technique, Sr Spec® resin (Eichrom Technologies, USA). Approximate 120 ng Sr from the sample is needed for Sr isotope analysis. The Sr isotopic composition of fluid samples was determined using a multi-collector inductively coupled plasma mass spectrometer (MC-ICP-MS, Neptune, Thermo Fisher Scientific) installed at Earth Dynamic System Research Center, National Cheng-Kung University. Both $^{87}Sr/^{86}Sr$ and $\delta^{88}Sr$ were measured with a modified empirical external normalization (EEN, Liu et al. 2012) coupled with traditional standard-sample-bracketing (SSB) technique. The reproducibility of

Table 1. Basic parameters and chemical composition of MV LS waters.

Sample name	Sampling date	Temperature (°C)	Gas flux (ml s^{-1})	Slurry flux (ml s^{-1})	pH	ORP (mV)	mud wt (%)	Cl^- (mM)	TA[c] (mM)	Na (mM)	Ca (mM)	Mg (μM)	B (μM)	K (μM)	Br (μM)	Si (μM)	Sr (μM)	S (μM)	Ba (μM)	Mn (μM)	Fe (μM)	I (μM)	Li (μM)
LS-A1_2002	2002-11-24		27					211		121	46.3	408	1030	376	271	156	68.6	38.3	6.40	31.1	0.05	13.8	11.9
LS-A1_2003[a]	2003-02-07		15					214		122	46.6	697	989	392	279	112	71.1	41.7	5.36	1.90	0.02	0.875	8.85
LS-A1_2003[b]	2003-02-07		20					217		122	46.4	683	987	427	292	94.8	71.2	41.4	5.54	3.00	-	1.27	8.76
LS-A1_2003[c]	2003-02-07		17					218		123	46.9	662	993	410	297	104	71.3	40.8	5.56	5.14	0.29	1.47	8.81
LS-A1_2008[a]	2008-12-14			26			15.6	228		123	47.4	465	898	336	285	107	71.6	19.9	4.01	23.4	0.03	11.4	11.1
LS-A1_2015-1[b]	2015-10-19	25.7			6.87	62	3.2	216	0.752	124	47.3	259	1020	342	293	153	67.3	37.1	4.90	7.06	0.04	12.7	12.1
LS-A1_2015-2[b]	2015-11-16	25.5			6.75	216	0.6	211	0.628	122	47.1	243	1010	329	289	212	66.8	36.8	4.76	7.22	-	12.6	11.9
LS-A1_2016-1[b]	2016-01-19	23.1	24	23	6.77	154	1.3	208	0.506	118	48.1	246	996	341	295	187	68.0	36.4	5.36	14.5	0.10	13.1	11.9
LS-A1_2016-2[b]	2016-02-23	23.7		30	6.54	167	1.8	218	0.477	119	47.8	256	996	321	292	166	68.5	36.1	5.28	13.9	0.07	3.08	12.0
LS-A1_2016-3[b]	2016-03-22	22.9	25	32	7.13	78	1.1	220	0.509	119	47.1	250	996	316	291	189	67.9	36.3	5.19	13.5	0.07	6.70	11.8
LS-A1_2016-4[b]	2016-04-26	26.1	47	20	7.30	-17	4.7	214	0.378	120	47.0	267	979	337	307	157	68.7	36.8	5.00	12.9	0.01	13.5	12.0
LS-A1_2016-5[b]	2016-05-24	26.1	22	19	6.90	-68	4.5	218	0.662	117	46.3	250	968	308	295	165	67.0	36.9	5.16	12.7	0.02	11.5	11.8
LS-A1_2016-6[b]	2016-06-21	27.6	24	31	7.02	-66	5.7	216	0.599	120	46.8	254	979	325	299	175	66.9	36.6	5.26	11.3	-	11.2	12.1
LS-A1_2016-7[b]	2016-07-19	31.0	33	23	6.97	-57	0.1	214	0.603	119	46.4	249	983	342	299	172	66.8	36.8	5.36	12.0	0.01	6.91	12.0
LS-A1_2017[b]	2017-01-16	24.3	3.6	20	7.23	-95	4.2	212	0.589	118	46.4	277	971	400	294	147	68.6	36.1	5.16	14.0	-	7.48	11.2
LS-A1_2018	2018-01-15	24.3		26	7.47	-136	35.1	219	0.332	116	46.4	236	897	330	335	90.4	66.0	36.8	4.90	6.81	0.05	9.61	11.1
LS-A1_2019	2019-01-04	26.2		25	7.03	-32	3.4	212	0.391	117	45.9	243	956	331	324	141	66.8	34.5	5.36	11.8	-	6.71	11.6
LS-A1_2020	2020-01-12	25.8	12	27	7.32	26	5.3	208	0.471	118	45.2	238	948	333	309	166	65.9	52.3	4.99	9.73	0.04	2.41	12.1
LS-A1_2021	2021-01-20	25.0	13	19	7.55	2	4.1	204	0.386	116	44.3	196	933	333	304	134	64.0	50.3	4.59	8.88	0.01	4.68	11.7
LS-A2_2008[a]	2008-12-14						48.0	227		123	48.2	365	909	313	285	110	69.4	24.1	4.99	24.8	0.01	12.1	13.4
LS-A3_2015-2	2015-11-16	24.9			6.72	-73	2.5	215	0.894	129	48.2	752	1040	202	295	249	59.8	37.7	3.25	47.0	29.2	9.84	1.47
LS-A3_2016-2	2016-02-23	18.9			7.03	150	0.1	220	0.900	121	47.7	957	1000	212	296	301	55.7	35.3	1.49	32.5	0.03	10.0	1.01
LS-A3_2016-3	2016-03-22	20.5			7.25	32	0.1	154	0.820	81	32.4	525	655	166	207	76.8	41.4	28.1	2.21	21.7	0.09	6.59	2.58
LS-A3_2016-5	2016-05-24	28.1			7.04	-44	14.6	210	1.07	114	43.8	777	909	276	288	93.6	54.8	34.3	3.38	40.7	0.42	10.3	1.16
LS-A3_2016-6	2016-06-21	28.3			7.13	-78	23.6	217	0.980	121	45.6	780	957	190	291	155	56.2	36.2	3.60	47.4	6.02	9.99	1.04
LS-A3_2016-7	2016-07-19	35.0			7.08	32	2.0	247	0.703	137	53.2	404	1140	356	333	149	74.9	44.6	5.56	19.0	0.02	8.90	11.5
LS-A3_2017	2017-01-16	19.7			7.23	-66	16.8	215	0.990	121	46.0	770	963	240	308	145	57.7	36.3	4.07	39.4	21.2	9.55	0.923
LS-A4_2016-1	2016-01-19	16.2			7.12	94	0.9	192	0.840	110	43.5	752	886	174	273	120	53.9	34.2	3.43	48.3	0.05	10.1	1.75
LS-A4_2016-3	2016-03-22	20.3			7.18	50	0.1	198	0.799	105	40.3	838	846	203	262	217	48.3	31.5	1.33	23.4	0.02	8.88	1.06
LS-A4_2016-5	2016-05-24	26.9			6.90	-45	10.8	210	1.32	115	43.9	900	917	213	295	210	53.4	34.7	1.56	38.5	5.10	13.9	1.02
LS-A4_2016-6	2016-06-21	30.8			7.06	-46	8.6	223	1.21	126	47.1	956	987	239	300	252	56.5	36.3	1.61	38.4	2.37	8.14	0.894
LS-A4_2016-7	2016-07-19	37.4			7.07	-14	0.1	233	1.06	133	49.6	991	1070	274	324	244	60.3	38.9	2.14	31.8	0.18	10.9	1.28
LS-A4_2017	2017-01-16	23.0			7.18	-22	0.5	216	1.15	122	46.1	947	981	301	305	339	55.3	35.7	1.44	30.2	-	8.08	0.966

Note: - not detected; blank: not determined. a: Data adopted from Chao et al. (2011) except concentration of K, Mn, and Fe as well as gas and slurry fluxes. b: Data adopted from Chao et al. (2022) except concentration of Br and I as well as gas and slurry fluxes. c: Based on the pH and the titration curve, most of the alkalinity contributed by bicarbonate.

Table 1. (Continued)

Sample name	Sampling date	Temperature (°C)	Gas flux (ml s^{-1})	Slurry flux (ml s^{-1})	pH	ORP (mV)	mud wt (%)	Cl^- (mM)	TA[c] (mM)	Na (mM)	Ca (mM)	Mg (μM)	B (μM)	K (μM)	Br (μM)	Si (μM)	Sr (μM)	S (μM)	Ba (μM)	Mn (μM)	Fe (μM)	I (μM)	Li (μM)
LS-A4_2018	2018-01-15	18.2			7.38	-57	0.5	226	0.883	121	46.5	908	968	293	316	314	58.4	36.0	1.18	35.0	0.03	8.86	1.25
LS-A4_2019	2019-01-04	24.8			7.16	77	0.3	208	0.928	118	44.6	909	951	259	308	314	55.8	33.7	1.16	33.6	-	9.02	1.12
LS-A4_2020	2020-01-12	22.5			7.60	57	0.1	214	0.845	122	45.0	908	966	261	320	294	55.5	51.7	1.15	29.7	0.08	4.70	1.29
LS-A5_2016-2	2016-02-23	18.6			7.04	-57	7.8	215	0.961	118	46.5	1150	933	140	289	232	46.4	35.0	2.53	45.0	3.15	11.0	0.352
LS-A5_2016-3	2016-03-22	19.9			7.14	-36	1.0	213	0.837	114	43.9	1090	883	132	289	233	44.9	33.7	2.05	44.4	0.22	12.6	0.329
LS-A5_2017	2017-01-16	20.2			7.19	-11	1.3	214	0.996	121	45.9	1140	948	209	304	216	47.1	35.8	2.58	43.0	17.1	7.56	0.366
LS-A6_2017	2017-01-16	21.1			7.03	-18	10.9	214	1.19	118	46.5	512	953	339	307	128	66.4	36.5	3.14	45.4	0.07	7.66	5.39
LS-A6_2018	2018-01-15	18.6			7.06	-34	0.5	230	1.14	119	48.3	656	933	349	325	117	67.8	38.9	3.56	73.4	0.08	10.9	4.39
LS-A6_2019	2019-01-04	24.0			7.12	-2	0.6	190	1.18	106	42.4	864	828	315	287	95.7	60.5	39.0	3.12	60.1	16.9	11.4	3.00
LS-B1_2002	2002-11-24							217		124	48.0	263	998	323	296	186	73.9	39.3	25.9	0.01	0.05	2.72	12.5
LS-B2_2021	2021-01-20	21.9			7.67	4	2.0	204	0.699	115	42.7	561	909	292	305	227	62.5	48.5	2.53	19.8	0.02	4.40	4.69
LS-D1_2002	2002-11-24		18					222		127	49.5	461	1100	437	299	85.7	79.0	92.7	5.71	0.13	0.13	0.467	9.32
LS-D1_2003	2003-09-21		57					148		81	31.3	295	700	249	200	249	51.3	27.7	13.9	0.27	0.27	3.36	8.93
LS-D1_2008[a]	2008-12-14			79			13.9	206		112	43.4	551	854	328	262	120	72.5	39.4	16.6	9.93	0.12	21.1	13.4
LS-D1_2017	2017-01-16	28.2		58	7.18	-57	2.6	209	0.598	118	45.7	346	981	390	304	221	76.2	35.7	22.4	5.67	-	8.30	12.6
LS-D1_2018	2018-01-15	27.6		54	7.04	119	11.4	217	0.470	116	45.4	352	933	386	306	162	74.5	36.1	23.7	3.47	0.01	11.3	12.4
LS-D1_2019	2019-01-04	29.2		62	7.24	-70	0.8	218	0.439	115	44.0	372	951	343	301	234	74.4	33.4	21.9	5.04	-	7.54	12.0
LS-D1_2020	2020-01-12	27.9		48	7.71	14	0.6	205	0.382	116	43.7	321	948	368	302	238	73.6	51.0	22.8	3.50	0.03	2.11	13.1
LS-D1_2021	2021-01-20	27.7		47	7.20	-24	1.3	194	0.419	110	41.0	281	872	328	291	201	69.0	46.8	19.9	2.89	0.01	6.21	11.3
LS-D2_2008[a]	2008-12-14						0.7	222		121	46.4	473	953	362	278	247	86.3	22.3	17.0	8.34	0.05	18.8	16.6
LS-D3_2002	2002-11-24							222		123	47.1	326	1110	404	291	85.4	72.7	47.5	18.3	0.03	-	1.26	9.61
LS-E1_2008[a]	2008-12-14						1.0	218		117	44.9	240	962	334	267	236	81.4	22.9	8.67	8.52	0.08	18.2	16.7
LS-E1_2017	2017-01-16	24.1			7.29	17	0.4	200	0.610	115	44.3	318	1000	374	289	262	80.6	34.5	10.3	7.61	-	6.25	13.5
LS-E1_2018	2018-01-15	24.0			7.40	131	0.7	207	0.445	111	43.6	329	980	361	294	225	78.0	34.8	10.1	8.01	0.03	9.53	13.6
LS-E1_2019	2019-01-04	25.1			7.17	22	0.2	209	0.404	112	42.7	295	976	332	291	250	78.0	31.9	9.46	7.21	-	6.12	13.1
LS-E1_2020	2020-01-12	22.9			7.45	65	0.4	197	0.475	113	42.4	298	977	346	296	271	77.9	49.5	9.43	6.82	0.03	3.45	13.7
LS-E1_2021	2021-01-20	21.7			7.04	33	0.2	196	0.424	111	41.5	246	935	329	285	256	75.3	46.6	8.16	6.32	0.02	4.79	12.5
LS-E2_2002	2002-11-24	21.1						228		129	45.1	1630	1140	580	295	80.7	141	91.0	8.17	2.88	0.21	4.12	13.0
LS-E3_2017	2017-01-16	23.9			7.34	35	0.5	199	0.610	114	44.2	217	1010	385	295	251	77.4	34.9	9.11	5.14	-	11.1	13.6
LS-E4_2021	2021-01-20				7.07	56	0.4	200	0.439	113	37.9	792	926	359	283	214	98.3	43.3	24.8	7.75	0.01	4.72	13.3
LS-F1_2002	2002-11-24							215		118	41.5	2840	959	622	272	111	174	42.3	26.4	0.05	0.20	1.99	15.2
LS-F1_2003	2003-09-21							214		116	41.4	2660	1030	561	272	167	144	38.6	109	2.21	0.07	1.35	15.2
LS-F1_2008[a]	2008-12-14			3.1			0.6	222		118	44.9	290	962	340	265	255	83.3	27.0	13.8	3.63	0.01	11.0	16.7
LS-F2_2008[a]	2008-12-14						0.6	212		118	44.7	292	953	319	269	295	81.7	27.8	8.37	5.81	0.02	14.1	16.9
LS-F3_2008[a]	2008-12-14						1.0	213		117	44.2	170	953	326	268	285	80.8	29.3	6.16	1.24	0.20	14.6	17.1

$^{87}Sr/^{86}Sr$ and $\delta^{88}Sr$ in international seawater standard IAPSO and in-house seawater LMN_4-3 is better than 0.000014 and 0.026‰ (2σ, n = 5) with the values of 0.709178, 0.378‰, and 0.709173, 0.380‰ respectively. The $\delta^{88}Sr$ results are expressed using conventional notation modified after Krabbenhöft et al. (2009):

$$\delta^{88}Sr = \left[\frac{^{88}Sr/^{86}Sr_{sample}}{^{88}Sr/^{86}Sr_{NBS\ SRM\ 987}} - 1 \right] \times 10^3\ (‰) \quad (2)$$

where $^{88}Sr/^{86}Sr_{sample}$ and $^{88}Sr/^{86}Sr_{standard}$ denote the $^{88}Sr/^{86}Sr$ ratio in the sample and standard respectively.

3. RESULTS

The concentration of major elements (Cl, Na, and Ca) from the water of mud pools in MV LS show similar results to previous reports (Yeh et al. 2005; Chao et al. 2011). The chemical composition sorted in order of the maximum molar concentration is Cl, Na, Ca, Mg, TA, B, K, Br, Si, Sr, Ba, S, Mn, Fe, I, Li, Al, Ni, Zn, Mo, Rb, Cu, As, Co, Ge, Ti, Sb, Cs, U, and Pb (Tables 1 and 2). The average concentration of three major elements is 211, 117, and 44.9 mM for Cl, Na, and Ca respectively. The sampled 5 groups show small variations of total dissolved solids (TDS) with the average value of 1.2% and are approximately 35% relative to seawater. According to the spatial and temporal variation, three categories of the dissolved components can be established: conservative, semi-conservative, and variable. Conservative components are Cl, Na, Ca, TA, B, Br, and S. Most of them are major elements. Semi-conservative components are Mg, K, Si, Sr, I, Al, Rb, Cu, Co, and Ti with variations less than an order. The rest of the chemical components are variable ones.

The measured O, H, and triple Sr isotopes also show similar patterns to previous studies (You et al. 2004; Yeh et al. 2005; Chao et al. 2013). The δD and $\delta^{18}O$ reveal small variation, and the values are slightly lower than those of seawater with the average by -1.7 and -0.37‰ respectively (Table 3). The mass independent $\Delta^{17}O$ has small negative fractionation with the average of -0.05‰. The 5 groups are not distinguishable from each other (Fig. 2). By excluding the high d-excess low chloride samples, which are diluted by meteoric water, and low d-excess high chloride samples, which result from evaporation, δD and $\delta^{18}O$ show no statistical differences among the 5 groups as well as the 6 mud pools in group A (Student's t test, $p > 0.05$). The overall correlation between δD and $\delta^{18}O$ has a slope of 2.12, possibly indicating a local evaporation line and similar to a previous study on MV LGH (Chao et al. 2022) as well as soil moisture (Dincer et al. 1974). Radiogenic Sr isotopes have igneous signal with small but detectable variation. The distribution of $^{87}Sr/^{86}Sr$ ratios are within 0.70653 and 0.70791 with an average value of 0.70684. Group A denotes lower $^{87}Sr/^{86}Sr$ ratios while groups D, E, and F have higher $^{87}Sr/^{86}Sr$ ratios with large variation before the year 2003 (Fig. 3). In contrast, group A has higher $\delta^{88}Sr$ with larger variation while the rest of the groups reveal lower $\delta^{88}Sr$ and smaller variation (Fig. 4). Stable Sr isotopes are distributed between 0.24 and 0.40‰ with an average value of 0.32‰.

4. DISCUSSION

4.1 Chemical and Isotopic Characteristic of Waters

In general, waters expelled by MVs reveal similar chemical characteristics to deep marine pore fluids. They originate from ancient seawater and are altered by early diagenesis, clay dehydration, and water-rock interaction (e.g., Dia et al. 1999; Dahlmann and de Lange 2003; Hensen et al. 2004; You et al. 2004; Mazzini et al. 2007, 2009; Ray et al. 2013; Farhadian Babadi et al. 2019; Chen et al. 2020). Seawater is an important reference for chemical and isotopic composition of MV waters and chloride is one of the most important dissolved components to decipher the source of the fluid besides seawater and the behavior of the elements. Both marine and terrestrial MVs generally contain lower chloride concentration, lower Mg/Cl, Ca/Cl, δD ratios with higher Na/Cl, B/Cl, Li/Cl, Ba/Cl, Br/Cl, I/Cl, $\delta^{18}O$ ratios compared with seawater (e.g., Dia et al. 1995; Lavrushin et al. 2003; Aloisi et al. 2004; Chao et al. 2011; Farhadian Babadi et al. 2019; Chen et al. 2020). MV LS reveals similar chemical and isotopic features except reverse relationship between Na/Cl and Ca/Cl (Table A1). The characteristic of higher Ca/Cl but lower Na/Cl ratios relative to seawater is usually indicated as low temperature (< 80°C) water-rock interaction with volcanic ashes or oceanic crust (Garlick and Dymond 1970; Seyfried and Bischoff 1979; Lawrence and Gieskes 1981; Henderson 1982) and has been observed in marine pore water (e.g., Gieskes et al. 1975, 1990; Perry et al. 1976; Lawrence and Gieskes 1981). The low $^{87}Sr/^{86}Sr$ ratio of the waters further supports this observation (Table 3; Fig. 3). MVs are geologic structures situated in thick sediment basins but waters of MV LS carries signals of igneous materials. This sediment-geothermal hybrid characteristic is named the sediment-hosted geothermal system (Procesi et al. 2019).

Besides Na/Cl and Ca/Cl ratios, MV LS shows Al/Cl, As/Cl, B/Cl, Ba/Cl, Co/Cl, Cu/Cl, Fe/Cl, Ge/Cl, Mn/Cl, Si/Cl, Sr/Cl ratios higher than those of seawater, Br/Cl, Cs/Cl, Li/Cl, Mo/Cl, Ni/Cl, Pb/Cl, Sb/Cl, TA/Cl, Ti/Cl, Zn/Cl ratios similar to those of seawater, and K/Cl, Mg/Cl, Rb/Cl, S/Cl, U/Cl lower than those of seawater (Table A1). The hydrothermal experiment (up to 350°C) of seawater and pelagic sediment indicates release of As, Cs, and Rb into the aqueous phase at high temperature (You et al. 1996). However, As/Cl shows slight higher, Cs/Cl shows similar, and Rb/Cl shows lower ratios than those of seawater, possibly

Table 2. Trace elements concentration in the range from pM to nM of MV LS waters.

Sample name	Al (nM)	Ti (nM)	Co (nM)	Ni (nM)	Cu (nM)	Zn (nM)	Ge (nM)	As (nM)	Rb (nM)	Mo (nM)	Sb (nM)	Cs (nM)	Pb (pM)	U (nM)
LS-A1_2002									123					0.16
LS-A1_2003[a]									136					1.2
LS-A1_2003[b]									152					1.5
LS-A1_2003[c]									136					1.4
LS-A1_2008[a]									101					0.97
LS-A1_2015-1	1200	3.8	11	12	41	36	4.7	25	172	13	2.2	3.6	25	0.43
LS-A1_2015-2	950	4.1	21	77	44	38	7.5	22	159	10	1.9	3.6	140	0.32
LS-A1_2016-1	1300	4.5	11	2.4	42	36	8.2	22	163	7.4	2.2	3.0	280	0.31
LS-A1_2016-2	2300	4.9	12	18	40	54	6.6	29	172	13	2.9	3.3	360	0.36
LS-A1_2016-3	2500	6.8	10	6.1	38	66	7.6	30	169	7.1	2.2	3.3	470	0.26
LS-A1_2016-4	1000	3.9	12	6.6	43	11	6.8	35	177	15	2.6	4.8	360	0.28
LS-A1_2016-5	570	4.4	12	4.1	39	10	6.8	32	139	5.0	1.4	2.7	250	0.23
LS-A1_2016-6	930	4.4	12	31	48	39	7.4	30	155	6.7	1.8	3.4	400	0.21
LS-A1_2016-7	840	4.7	11	21	43	32	8.8	28	175	7.0	1.7	3.6	210	0.24
LS-A1_2017	370	5.5	9.3	44	42	7.5	6.2	33	157	8.5	1.8	2.9	390	0.22
LS-A1_2018	470	4.4	13	20	43	7.3	5.8	29	160	25	4.1	2.6	64	0.28
LS-A1_2019	740	3.7	11	21	41	10	7.8	26	172	7.0	1.5	2.5	190	0.21
LS-A1_2020	1900	4.8	13	31	41	100	5.8	21	155	8.1	1.7	2.8	450	0.22
LS-A1_2021	630	4.1	13	56	39	90	4.5	30	160	10	2.2	2.6	440	0.22
LS-A2_2008[a]									97.5					1.0
LS-A3_2015-2	2100	4.4	20	1.0	35	62	1.3	36	44.0	30	0.52	0.87	48	0.60
LS-A3_2016-2	520	5.6	15	2.0	66	11	1.1	71	24.4	41	2.0	0.56	51	0.46
LS-A3_2016-3	2900	4.4	13	14	32	75	1.1	29	34.2	20	0.92	0.43	63	0.79
LS-A3_2016-5	770	4.9	15	2.7	39	8.8	1.3	33	21.1	33	0.67	0.34	17	1.1
LS-A3_2016-6	900	4.2	18	3.1	40	25	1.3	40	47.5	41	0.59	0.80	17	0.75
LS-A3_2016-7	880	3.2	21	17	78	20	3.6	32	142	20	2.7	1.5	99	0.73
LS-A3_2017	480	4.1	17	2.1	39	18	1.4	55	39.4	55	1.2	0.50	75	0.90
LS-A4_2016-1	690	2.9	28	23	60	20	1.1	25	51.1	33	1.2	1.0	68	1.3
LS-A4_2016-3	1400	4.9	14	2.6	68	49	1.0	34	26.6	39	3.2	0.56	250	0.72
LS-A4_2016-5	570	5.0	20	2.7	37	9.7	1.3	48	19.9	44	1.4	0.21	26	0.93
LS-A4_2016-6	1600	5.8	21	2.0	41	58	1.3	62	25.0	42	1.2	0.40	28	0.67
LS-A4_2016-7	630	5.7	26	12	110	34	1.7	48	51.2	63	4.2	0.77	200	0.64
LS-A4_2017	570	6.0	17	2.1	66	30	1.6	57	30.7	42	2.2	0.85	180	0.44
LS-A4_2018	220	9.6	21	12	73	15	1.5	40	31.5	38	2.9	0.45	160	0.41
LS-A4_2019	790	5.5	20	15	77	28	1.5	48	29.9	37	1.3	0.36	90	0.37
LS-A4_2020	420	10	21	28	88	160	1.4	71	29.4	34	1.8	0.55	70	0.28
LS-A5_2016-2	1800	5.8	21	2.3	50	26	1.0	44	20.0	40	1.0	0.31	44	0.46
LS-A5_2016-3	1000	5.4	22	2.1	66	35	1.0	36	23.8	46	0.82	0.50	22	0.30
LS-A5_2017	1100	5.5	20	2.7	42	77	1.2	35	23.7	42	1.9	0.29	57	0.59
LS-A6_2017	750	5.4	14	2.3	45	7.9	1.4	23	68.5	17	0.72	0.90	48	0.50
LS-A6_2018	740	4.8	36	61	78	18	1.4	31	67.5	25	5.5	1.2	230	2.6
LS-A6_2019	570	3.7	26	35	35	8.9	1.3	56	29.4	23	5.4	0.19	40	2.2
LS-B1_2002									164					0.45
LS-B2_2021	640	4.3	16	28	39	6.9	2.0	80	54.0	33	5.5	0.70	270	0.51
LS-D1_2002									162					1.4
LS-D1_2003									144					0.42
LS-D1_2008[a]									111					2.1
LS-D1_2017	470	6.2	11	1.6	47	16	10	28	171	9.3	2.1	1.3	290	0.31
LS-D1_2018	1400	5.1	11	2.3	40	51	6.8	39	175	23	4.9	1.3	150	0.55

Note: blank: not determined. a: Data adopted from Chao et al. (2011).

Table 2. (Continued)

Sample name	Al (nM)	Ti (nM)	Co (nM)	Ni (nM)	Cu (nM)	Zn (nM)	Ge (nM)	As (nM)	Rb (nM)	Mo (nM)	Sb (nM)	Cs (nM)	Pb (pM)	U (nM)
LS-D1_2019	710	4.7	13	5.1	41	21	12	33	180	10	2.2	1.6	150	0.33
LS-D1_2020	2100	5.3	13	15	41	150	11	35	188	8.3	2.1	2.0	310	0.16
LS-D1_2021	440	4.2	14	26	42	50	13	38	180	15	2.9	2.0	200	0.39
LS-D2_2008 [a]									176					0.39
LS-D3_2002									123					2.0
LS-E1_2008 [a]									119					0.46
LS-E1_2017	450	5.4	17	14	43	19	22	24	132	7.9	0.66	2.6	130	0.091
LS-E1_2018	890	4.8	23	91	45	13	20	35	137	21	3.5	2.9	600	0.21
LS-E1_2019	660	5.8	16	10	43	15	23	26	137	7.4	0.52	2.7	150	0.067
LS-E1_2020	2000	6.3	24	83	43	120	18	28	139	10	0.88	2.9	360	0.10
LS-E1_2021	520	4.9	13	15	42	18	18	30	134	6.2	0.60	2.7	170	0.058
LS-E2_2002									140					2.2
LS-E3_2017	700	5.4	16	37	68	18	33	25	121	7.9	0.79	1.9	260	0.069
LS-E4_2021	720	5.0	23	81	41	82	23	27	118	12	1.4	2.1	530	0.18
LS-F1_2002									219					1.8
LS-F1_2003									193					1.0
LS-F1_2008 [a]									147					0.15
LS-F2_2008 [a]									186					0.17
LS-F3_2008 [a]									177					0.10

Table 3. Isotopic composition of MV LS waters.

Sample name	δD (‰)	$\delta^{18}O$ (‰)	d-excess[c] (‰)	$\Delta^{17}O$ (‰)	$^{87}Sr/^{86}Sr$	2 SD n = 3	$\delta^{88}Sr$ (‰)	2 SD n = 3
LS-A1_2002					0.70679	0.00002	0.30	0.01
LS-A1_2003[a]					0.70685	0.00001	0.29	0.01
LS-A1_2003[b]					0.70686	0.00002	0.28	0.01
LS-A1_2003[c]					0.70686	0.00003	0.29	0.05
LS-A1_2008[a]	-1.4	-0.5	2.7		0.70684	0.00003	0.31	0.01
LS-A1_2015-1[b]	-3.0	-0.43	0.5	-0.04	0.70678	0.00001	0.32	0.02
LS-A1_2015-2[b]	-2.9	-0.65	2.3	-0.03	0.70678	0.00005	0.32	0.01
LS-A1_2016-1[b]	-2.0	-0.12	-1.0	-0.02	0.70678	0.00001	0.34	0.02
LS-A1_2016-2[b]	-1.5	0.07	-2.0	-0.03	0.70678	0.00001	0.30	0.01
LS-A1_2016-3[b]	-3.7	-0.68	1.8	-0.04	0.70677	0.00004	0.32	0.03
LS-A1_2016-4[b]	-3.0	-0.45	0.5	-0.07	0.70676	0.00002	0.29	0.02
LS-A1_2016-5[b]					0.70678	0.00002	0.32	0.02
LS-A1_2016-6[b]	-2.2	-0.48	1.7	0.01	0.70679	0.00002	0.34	0.02
LS-A1_2016-7[b]	-2.2	-0.70	3.4	-0.10	0.70679	0.00002	0.33	0.02
LS-A1_2017[b]	-2.5	-0.35	0.4	-0.05	0.70683	0.00003	0.31	0.01
LS-A1_2018	-2.4	-0.58	2.3	-0.03	0.70679	0.00001	0.33	0.02
LS-A1_2019	-2.2	-0.67	3.2		0.70678	0.00003	0.30	0.01
LS-A1_2020	-2.5	-0.53	1.8		0.70676	0.00002	0.35	0.02
LS-A2_2008 [a]	-2.0	-0.7	3.5		0.70678	0.00004	0.28	0.02
LS-A3_2015-2	-0.5	0.04	-0.8	-0.06	0.70673	0.00003	0.39	0.01
LS-A3_2016-2					0.70667	0.00001	0.37	0.01
LS-A3_2016-3	-0.8	-1.46	10.9	-0.01	0.70677	0.00001	0.39	0.01
LS-A3_2016-5	-3.5	-0.73	2.3	-0.10	0.70671	0.00005	0.36	0.02
LS-A3_2016-6	-2.2	-0.45	1.4	-0.01	0.70673	0.00003	0.37	0.01

Note: blank: not determined. a: Data adopted from Chao et al. (2013). b: Data adopted from Chao et al. (2022). c: deuterium excess = $\delta D - 8 \times \delta^{18}O$.

Table 3. (Continued)

Sample name	δD (‰)	$\delta^{18}O$ (‰)	d-excess[c] (‰)	$\Delta^{17}O$ (‰)	$^{87}Sr/^{86}Sr$	2 SD n = 3	$\delta^{88}Sr$ (‰)	2 SD n = 3
LS-A3_2016-7	-0.8	0.39	-3.9	-0.13	0.70678	0.00002	0.32	0.03
LS-A3_2017	-0.9	-0.25	1.1	-0.05	0.70670	0.00001	0.37	0.01
LS-A4_2016-1	-0.2	-0.50	3.9	0.01	0.70673	0.00001	0.36	0.02
LS-A4_2016-3	-2.4	-0.79	3.9	-0.06	0.70667	0.00001	0.36	0.02
LS-A4_2016-5	-4.2	-0.84	2.5	-0.04	0.70667	0.00003	0.37	0.01
LS-A4_2016-6	-0.2	0.03	-0.5	-0.08	0.70670	0.00001	0.37	0.01
LS-A4_2016-7	0.3	0.55	-4.1	0.01	0.70667	0.00003	0.39	0.01
LS-A4_2017	0.0	0.25	-2.0	-0.11	0.70667	0.00003	0.37	0.02
LS-A4_2018	-0.1	-0.12	0.9	-0.05	0.70670	0.00003	0.34	0.01
LS-A4_2019	-2.2	-0.85	4.7		0.70669	0.00002	0.37	0.02
LS-A4_2020	0.9	0.07	0.3		0.70675	0.00005	0.32	0.01
LS-A5_2016-2	0.4	0.84	-6.4	-0.04	0.70653	0.00002	0.40	0.01
LS-A5_2016-3	-3.1	-0.58	1.6	-0.08	0.70654	0.00002	0.38	0.01
LS-A5_2017	-1.0	-0.37	2.0	-0.03	0.70653	0.00003	0.40	0.03
LS-A6_2017					0.70680	0.00005	0.30	0.01
LS-A6_2018	3.6	0.45	0.0	-0.02	0.70678	0.00001	0.31	0.02
LS-A6_2019	-2.5	-1.33	8.1		0.70682	0.00002	0.32	0.01
LS-B1_2002					0.70683	0.00001	0.28	0.01
LS-D1_2002					0.70691	0.00002	0.28	0.01
LS-D1_2003					0.70690	0.00001	0.28	0.02
LS-D1_2008[a]	-1.8	-0.5	2.3		0.70689	0.00002	0.27	0.02
LS-D1_2017					0.70692	0.00002	0.29	0.01
LS-D1_2018	-1.9	-0.41	1.4	-0.02	0.70690	0.00001	0.26	0.01
LS-D1_2019	-2.7	-0.77	3.5		0.70693	0.00002	0.27	0.01
LS-D1_2020	-2.3	-0.53	1.9		0.70691	0.00005	0.28	0.02
LS-D2_2008[a]	-0.8	-0.3	1.6		0.70705	0.00004	0.26	0.01
LS-D3_2002					0.70682	0.00002	0.29	0.02
LS-E1_2008[a]	-0.6	-0.1	0.5		0.70690	0.00002	0.30	0.02
LS-E1_2017	-1.8	0.05	-2.3	-0.04	0.70694	0.00002	0.27	0.01
LS-E1_2018	-2.4	-0.40	0.9	-0.06	0.70692	0.00002	0.24	0.01
LS-E1_2019	-2.5	-0.62	2.5		0.70693	0.00002	0.30	0.02
LS-E1_2020	-2.3	-0.43	1.2		0.70690	0.00002	0.29	0.02
LS-E2_2002					0.70755	0.00002	0.28	0.01
LS-E3_2017	-2.5	-0.43	0.9	-0.06	0.70690	0.00002	0.27	0.01
LS-F1_2002					0.70791	0.00002	0.25	0.03
LS-F1_2003					0.70773	0.00001	0.26	0.03
LS-F1_2008[a]	0.0	0.0	0.0		0.70693	0.00002	0.28	0.02
LS-F2_2008[a]	-1.4	-0.3	1.3		0.70691	0.00002	0.26	0.02
LS-F3_2008[a]	-0.6	-0.1	0.3		0.70691	0.00001	0.28	0.01

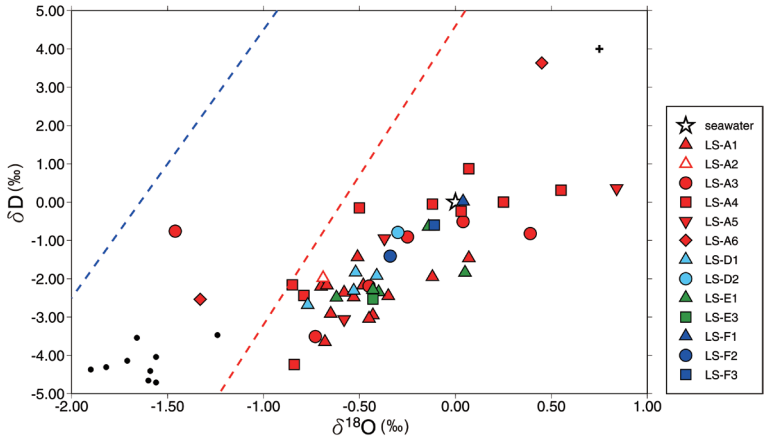

Fig. 2. Plot of δD vs $\delta^{18}O$ for all MV waters in this study. Seawater composition, igneous end member of MV LGH (dots; Chao et al. 2022), and local meteoric water line (Peng et al. 2010) show for reference. Blue dash line denotes local meteoric water line of the winter monsoon and red dash line denotes the summer monsoon. The cross denotes the range of the reproducibility (2σ). The slope of increasing trend is approximately 2, possibly implying local evaporation line.

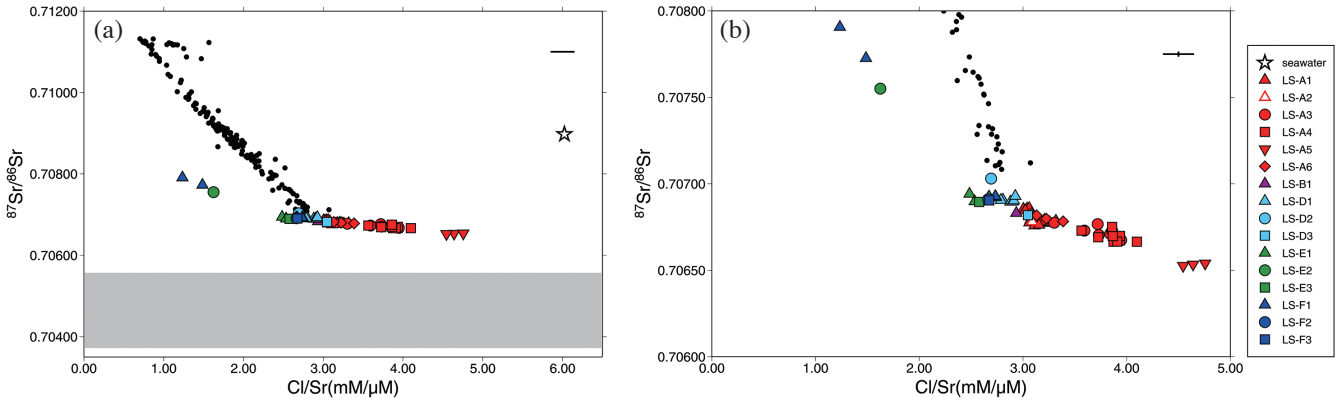

Fig. 3. Plot of $^{87}Sr/^{86}Sr$ vs Cl/Sr ratio for all MV waters in this study. (a) Seawater composition, MV LGH (dots; Chao et al. 2022), and the arc basement (andesite; shaded area) show for reference. (b) Zoom in to focus on MV LS. The range of the cross denotes the range of the reproducibility (2σ). The range of andesite $^{87}Sr/^{86}Sr$ is adopted from Chen et al. (1990) and Bentahila et al. (2008). Variation of the ancient seawater since 5 Ma is smaller than the symbol.

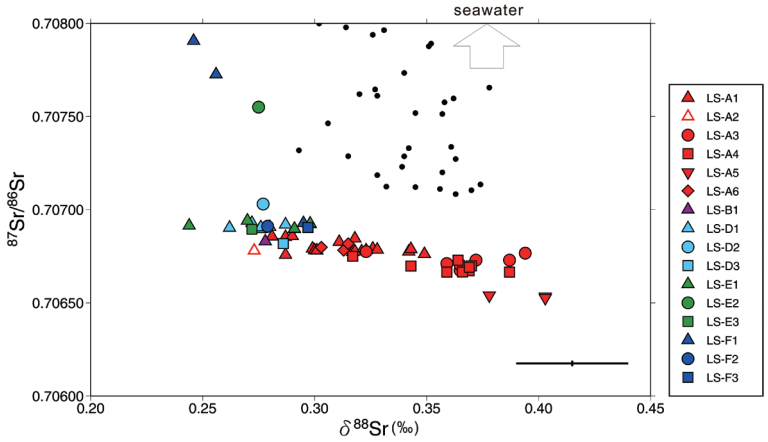

Fig. 4. Plot of $^{87}Sr/^{86}Sr$ vs $\delta^{88}Sr$ for all MV waters in this study. Seawater composition is not in the figure. Data of MV LGH (dots; Chao et al. 2022) shows for reference. The range of the cross denotes the range of the reproducibility (2σ).

resulting from lower formation temperature than that of hydrothermal experiments. The formation temperature of MV LS fluid is between 79 and 98°C, determined by various chemical geothermometers (Chao et al. 2011). The field investigation of low-temperature (62 to 64°C) ridge-flank hydrothermal springs reveals that the concentrations of Co, Mn, Mo, Ni, and Zn are greater in the hydrothermal fluid than in bottom seawater while alkalinity, Cu, K, Li, Mg, Na, Rb, and U are lower (Wheat and Mottl 2000; Wheat et al. 2002). The low-temperature deep sea springs show more similar characteristic to MV LS. Due to elevated temperature, the greater water-rock interaction results in higher Al/Cl, Ba/Cl, Ge/Cl, Si/Cl, and Sr/Cl ratios but lower K/Cl, Mg/Cl, Na/Cl, and Rb/Cl in the water. Cs is more mobile than Rb. That may explain a higher Cs/Cl ratio than Rb/Cl compared to that of seawater. Besides water-rock interaction, the temperature enhances organic matter decomposition and leads to high B/Cl and I/Cl ratios (e.g., Ullman and Aller 1983; You et al. 1993). The high B/Cl ratio is also contributed by desorption of B from clays (e.g., You et al. 1993; Chao et al. 2011). Mn and U are caused by the change of redox condition. The low ORP (Table 1) indicates reducing condition in MV waters, thus, releases Mn into but precipitates U out of the water. The characteristic of Cu shows conflicting results between low-temperature deep sea springs and MV LS. The concentration of Cu in the springs is lower than that of bottom seawater and inferred as being precipitated into sulfide phase (Wheat and Mottl 2000; Wheat et al. 2002). The concentration of S in MV LS is low due to strong anaerobic oxidation of methane (AOM; Chang et al. 2012). Low S may result in higher Cu content in the MV water.

The results of δD, $\delta^{18}O$, and $\Delta^{17}O$ are slightly lower than present seawater (Table 3). Yeh et al. (2005) indicate that these low isotopic values are contributed by meteoric water. However, local meteoric water shows strong seasonal variation and the average value of all seasons are lower than that of MV waters (Peng et al. 2010). Additionally, major elements Cl, Na, and Ca as well as δD, $\delta^{18}O$, and $^{87}Sr/^{86}Sr$ in the MV water reveal minor variations, indicating a single and consistent source of MV LS. Meteoric water has positive $\Delta^{17}O$ (Sharp et al. 2018; Aron et al. 2021), but results of MV LS water show negative fractionation. The evidence implies that meteoric water is not likely to be the source of MV LS water. Chao et al. (2022) propose a three-step model for the origination of the MV waters in eastern Taiwan to explain the lower Cl^-, δD, and $\delta^{18}O$ relative to seawater. In brief, eastern Taiwan MV waters originate from the ancient seawater approximately 5 to 6 Ma, estimated by initial deposition age of forearc basin (e.g., Chang et al. 2000; Lin et al. 2019). The $\delta^{18}O$ decreases probably down to -9 or -12‰, and Cl^- is slightly diluted by water-rock interaction with volcanic ashes or andesitic basement. At final stage, $\delta^{18}O$ increases on account of clay dehydration fluid and couples with further chloride dilution at the source region.

The results of $\Delta^{17}O$ in MV water reveal negative fractionation, ranging from -0.13 to 0.01‰ (Fig. 5). This range falls in the region of pore water evolution curve (Sengupta and Pack 2018; Sengupta et al. 2020) and hydrothermal alternated rocks (Sharp et al. 2018). The curve indicates water-rock interaction with low temperature sediments (Sengupta and Pack 2018; Sharp et al. 2018). MVs are diapir structures in thick sediment basins, and MV LS is situated by a mountain with andesite basement. Both water-rock interaction with sediments and hydrothermal alternated rocks may result in low $\Delta^{17}O$. However, the results of $^{87}Sr/^{86}Sr$ in MV water reveal igneous characteristic and support the conclusion that hydrothermal alternated rocks have a better chance of fractionating oxygen.

4.2 The Mechanisms of Spatial and Temporal Variation

4.2.1 Spatial Distribution

Due to limited variation of Cl, Na, Ca, δD, and $\delta^{18}O$ in the waters of MV LS temporally and spatially, all the mud pools in MV LS may have similar or the same source region. The variation and the difference of trace elements among mud pools may be brought about by other secondary factors or the locality of the fluid reservoir on a smaller scale. Radiogenic Sr isotopes, $^{87}Sr/^{86}Sr$, are robust tracers for water mass studies, including groundwater, seawater, river water as well as MV waters (e.g., Land et al. 2000; Chung et al. 2009; Huang et al. 2011; Chao et al. 2013) and may help to decipher small differences in the source. In the dissolved phase, high $^{87}Sr/^{86}Sr$ ratio is often interpreted as the signal of sediment rock (e.g., > 0.710) and low ratio is igneous rock (e.g., < 0.707). Seawater is another important end member and has its value at around 0.7091. Waters in MV LS have $^{87}Sr/^{86}Sr$ variation between 0.70653 and 0.70791, indicating strong signature of water-rock interaction with igneous rock. After chloride normalization to remove the effect of dilution and evaporation, $^{87}Sr/^{86}Sr$ has a strong negative correlation with Cl/Sr ratio (Fig. 3). Even without normalization, $^{87}Sr/^{86}Sr$ has high positive correlation with Sr concentration in the waters of MV LS ($r = 0.97$; Table A2). Southern groups D, E, F have high $^{87}Sr/^{86}Sr$ with high Sr concentration. Mud pools at group A show lower $^{87}Sr/^{86}Sr$ and Sr concentration distribution. Mud pools LS-A1, LS-A2, and LS-A6 show similar $^{87}Sr/^{86}Sr$ as well as group B. Mud pools LS-A3 and LS-A4 have similar $^{87}Sr/^{86}Sr$ but lower than that of LS-A1. Mud pool LS-A5 has the lowest $^{87}Sr/^{86}Sr$ but still higher than that of andesite basement ($^{87}Sr/^{86}Sr = 0.70372$ to 0.70557; Chen et al. 1990; Bentahila et al. 2008; Fig. 3).

The spatial distribution of $^{87}Sr/^{86}Sr$ indicates the addition of high $^{87}Sr/^{86}Sr$ and high Sr water in the southern part of MV LS. Both sediment interacted water and seawater have higher $^{87}Sr/^{86}Sr$ than MV LS. The positive correlation

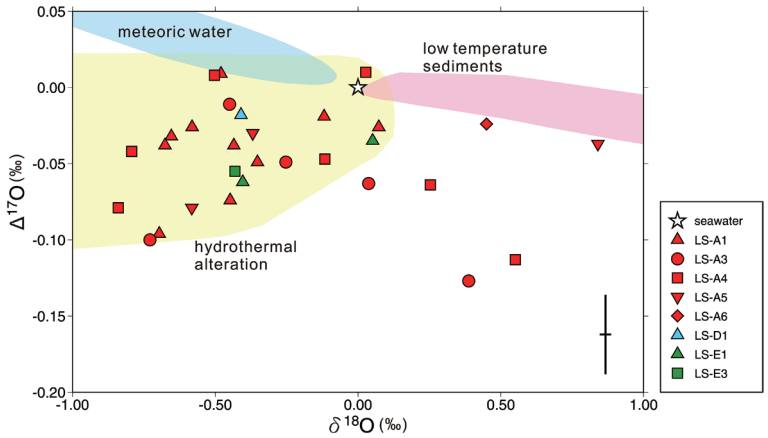

Fig. 5. Plot of $\Delta^{17}O$ vs $\delta^{18}O$ for all MV waters in this study. Seawater composition and the distribution of meteoric water, hydrothermal alteration and low temperature sediments (Sharp et al. 2018) show for reference. The range of the cross denotes the range of the reproducibility (2σ).

between $^{87}Sr/^{86}Sr$ and Sr concentration is similar to waters at MV LGH, which is inferred as two end member mixing of sedimentary and igneous sources (Chao et al. 2022). But $^{87}Sr/^{86}Sr$ and Sr distribution in MV LGH are much larger than that of MV LS. The highest value of $^{87}Sr/^{86}Sr$ in LGH waters exceeds 0.71132, absolutely contributed by sediments (Fig. 3). The preservation of ancient seawater is a possible source of the rise in $^{87}Sr/^{86}Sr$ as well as Sr content in the water. However, seawater composition does not fall on the extrapolating mixing line (Fig. 3). Additionally, $\delta^{88}Sr$ has negative correlation with $^{87}Sr/^{86}Sr$ (Fig. 4). Seawater has $\delta^{88}Sr$ as high as 0.38‰ presently. Considering the age, the reported ancient seawater of maximum deposition age 5 to 6 Ma (e.g., Chang et al. 2000; Lin et al. 2019) has the value between 0.340 to 0.375‰ (Paytan et al. 2021). The addition of preserved ancient seawater will raise or keep $\delta^{88}Sr$ of MV waters and this interpretation conflicts with what the results indicate. Sediments have low $\delta^{88}Sr$ (down to -0.2‰; Halicz et al. 2008; Chao et al. 2015). River water and groundwater have $^{87}Sr/^{86}Sr$, Sr/Cl, and Mg/Cl ratios higher than MV LS waters and is a possible source if they mix with MV waters at near surface. However, LS-D1_2003, which shows chloride concentration 33% lower than other MV waters, is diluted by surface runoff from nearby rice paddy (Table 1). The $^{87}Sr/^{86}Sr$ ratio of LS-D1_2003 reveals no variation compared with other LS-D1 samples because Sr concentration in MV waters is too high to vary $^{87}Sr/^{86}Sr$ by surface water addition. Thus, sediment interacted water has low $\delta^{88}Sr$ with high $^{87}Sr/^{86}Sr$, which leads to negative correlation with $^{87}Sr/^{86}Sr$ and $\delta^{88}Sr$ (Chao et al. 2022). Therefore, the slight addition of sedimentary water at groups D, E, and F or the rock that hosts the reservoir of the fluid containing higher potion of sediments are the possible explanations of the rise in $^{87}Sr/^{86}Sr$ and Sr but the drop in $\delta^{88}Sr$ in the MV waters. The spatial distribution of high $^{87}Sr/^{86}Sr$ samples, which were collected from the southern groups, may indicate where the sedimentary water is hosted. Although the trend of $^{87}Sr/^{86}Sr$ versus Cl/Sr ratios is similar for MV LGH and LS, the extrapolated mixing lines indicate that the sedimentary end members are different in two MVs (Fig. 3).

Pearson's correlation between $^{87}Sr/^{86}Sr$ and other chemical parameters (Table A2) is able to further determine the elements which are dominated by the source. The results indicate positive high correlation with Sr, K, and Ge, positive moderate correlation with Mg, Li, Ba, Rb, Cs, and Pb, negative high correlation with Mo, and negative moderate correlation with TA, Mn, and $\delta^{88}Sr$. The positive correlation with Sr, Mg, Li, Ba, and the negative correlation with $\delta^{88}Sr$ are consistent with waters from MV LGH (Chao et al. 2022). However, the source also causes great variation of major elements, Na and Ca, in LGH waters, but they have only minor variation and are considered conservative elements in MV LS. This discrepancy probably results from the proportion of the mixing. Sedimentary water contributes more to MV LGH than to MV LS. More contribution leads to variation of major elements. The contribution to MV LS is small and can only cause the trace elements and Sr isotopes, which are more sensitive to the source, to vary.

The second cluster of correlated elements is chloride related elements. Chloride has high positive correlation with B, Br, Ca, Na, moderate positive correlation with $\delta^{18}O$ and temperature, high negative correlation with d-excess (Table A2). B, Br, Ca, and Na are conservative elements in MV LS water. Negative correlation between d-excess and $\delta^{18}O$ as well as temperature indicates this cluster is evaporation varied elements. Another interesting correlation is moderate negative correlation between ORP and mud weight. This correlation may result from the intensity of gas bubbling or gas flux. The strong bubbling mixes mud breccia and water in the pool well and thus increases the percentage of mud in the sampling tube and enhances the AOM due to high methane support as well as reduces the ORP. Low gas

flux results in the settling down of mud breccia in the pool, decreasing the proportion of mud in the sampling tube, and increasing ORP by weaker AOM.

4.2.2 Temporal Variation

The temporal variation of $^{87}Sr/^{86}Sr$ was notably different in mud pools at groups E and F from which samples were collected before the year 2004 (Fig. 6). LS-F1_2002 had the highest $^{87}Sr/^{86}Sr$ ratio among all samples, and the ratio dropped sharply down to a similar value to group D before the year 2008 investigation. Mud pool LS-E2 was dead before the year 2003 investigation; therefore, it is not meaningful to discuss the variation. Group F is a swamp-like mud volcano and located on a boggy mudstone hill. The formation is loose, the hill is fracture rich (Chao et al. 2010), and the location is at the southernmost of the MV field. These characteristics make group F more sensitive to geological stress variation or additional fluids than other groups. A major earthquake, the Chengkung earthquake Mw = 6.8, happened on 10th December 2003. Strong fluid expulsion at LS-A1 after the earthquake is reported (Jiang et al. 2011) and a co-seismically unclamping fluid channel is indicated (Bonini et al. 2016; Bonini 2021). After the earthquake, groups E and F reveal similar $^{87}Sr/^{86}Sr$, K, Mg, and Sr to group D (Fig. 6), possibly indicating the waters originate from the same reservoir. As described in section 4.2.1, the mixing trend established by groups E and F before the year 2003 may result from minor sedimentary water addition and the earthquake has closed the pathway of sedimentary water to groups E and F. The higher and stable $^{87}Sr/^{86}Sr$ of groups D, E, and F after the year 2008 may have resulted from different fluid reservoir from group A. The fluid reservoir of groups D, E, and F may situate in a place whose ambient rock contains higher $^{87}Sr/^{86}Sr$ than group A's.

Most long-lasting mud pools show nearly no temporal variations on $^{87}Sr/^{86}Sr$ and major elements (e.g., LS-D1 and LS-E1). Except Cu and Rb, all the other trace elements, including Si and I, whose concentration are above μM level, reveal large variation for mud pools with constant $^{87}Sr/^{86}Sr$. This phenomenon indicates that those elements may be varied by fluid migration, biological activity, or other secondary factors and are not suitable for source identification. LS-A1 has a small but detectable increased $^{87}Sr/^{86}Sr$ in the years 2003 and 2008 samples (Fig. 6). LS-A2 is different from other satellite mud pools like LS-A3 to LS-A6, and it is like a twin mud pool of LS-A1 in the year 2008 (Fig. 1d). Evidence of other source related elements indicates that LS-A2_2008 is chemically and isotopically closer to LS-A1_2015-1 and the samples after (Table 3; Fig. 6). In the year 2003, LS-A1 emitted waters containing slightly more sedimentary contribution. This water has higher $^{87}Sr/^{86}Sr$, Mg, K but lower Li. In the year 2008, LS-A1 splits into twins: LS-A1_2008 and LS-A2_2008. LS-A2_2008 has lower $^{87}Sr/^{86}Sr$, Mg, K but higher Li and closer to LS-A1_2002 and LS-A1_2015-1 than LS-A1_2008, indicating the source of LS-A2_2008 has taken over LS-A1. The small variation of $^{87}Sr/^{86}Sr$, K, Mg, and Li may not represent the change of the source but the vibration of the reservoir. Mg shows more variation (250%) than K (20%) and other major elements such as Cl, Na, and Ca show no variation (Table 1 and A1). During the fluid migration, Mg has shorter re-equilibrium time than K and Na (Giggenbach 1988; Verma et al. 2008). If the fluid has stopped in the underground reservoir on a longer timescale, Mg concentration will fluctuate owing to new condition of water-rock interaction such as temperature or lithology. Therefore, the increase in Mg, K, and $^{87}Sr/^{86}Sr$ may have resulted from the move of reservoir or the change of fluid residence time. Neither gas nor slurry fluxes show significant difference during the entire study period (Table 1). Although flux measurement did not conduct on the year 2008, the photo indicates similar gas bubbling area and mud overflow condition comparing to other period (Fig. 1d). The vibration of the reservoir location or the size is the plausible mechanism for the chemical and isotopic variation of LS-A1.

By comparing the major mud pool in group A, LS-A1, with satellite mud pools (i.e., LS-A3 to LS-A6), LS-A5 is found to have the lowest $^{87}Sr/^{86}Sr$ and Sr, Li, K concentration with highest Mg concentration. LS-A3, LS-A4, and LS-A6 are distributed in between. The relationship of temporal variation indicates LS-A1 and LS-A3 have reversed direction of chemical variation on Mg and Li with $^{87}Sr/^{86}Sr$ (Fig. 6). Previously described increasing $^{87}Sr/^{86}Sr$ coupled with increasing Mg and decreasing Li of LS-A1 has reverse trend of LS-A3 as well as the relationship between LS-A3 and LS-A5. These chemical characteristics may imply that LS-A1 and LS-A5 originate from different fluid reservoirs. The water in LS-A5 reservoir has longer residence time as indicated by very low fluid flux. The flux is too low to be measured on site.

LS-A3 and LS-A4 show similar $^{87}Sr/^{86}Sr$ and trace elements such as K, Mg, Li, and Rb but LS-A3 has larger temporal variation. LS-A3_2016-3 and LS-A3_2016-7 have similar $^{87}Sr/^{86}Sr$ and trace elements to LS-A1, possibly due to the invasion of LS-A1 water into the LS-A3 channel near surface. The relationship of LS-A1, LS-A3, LS-A4, and LS-A5 reveal that the waters of LS-A3 and LS-A4 are resulted from the mixing of LS-A1 and LS-A5. LS-A6 has similar and constant $^{87}Sr/^{86}Sr$ to LS-A1 but trace elements show great discrepancy with LS-A1 as well as large temporal variation such as Mg, Li, B, Cu, and Rb (Fig. 6). The trend of temporal variation moves from concentration close to LS-A1 toward LS-A5. The chemical discrepancy between LS-A1 and LS-A6 may denote the origination of the same reservoir but split fluid channels at depth. Temporal variation of trace elements (e.g., Mg and Li) indicates the water of LS-A6 is gradually influenced by similar secondary mechanism that affects LS-A3, LS-A4, and LS-A5.

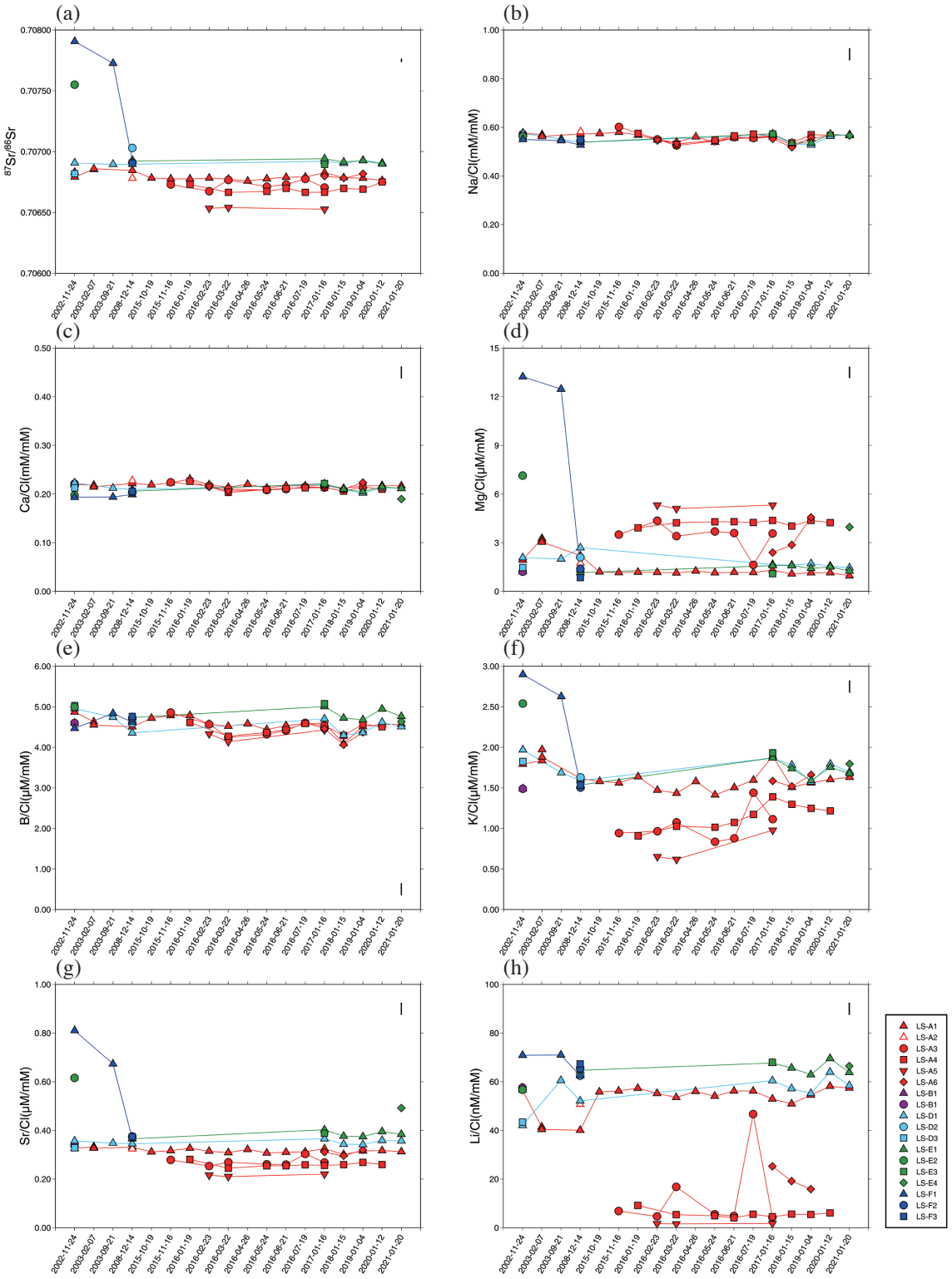

Fig. 6. Plot of the 19-year temporal variation of all MV LS waters for (a) $^{87}Sr/^{86}Sr$, (b) Na/Cl, (c) Ca/Cl, (d) Mg/Cl, (e) B/Cl, (f) K/Cl, (g) Sr/Cl, (h) Li/Cl ratios. The range of the bar denotes the range of the reproducibility (2σ).

The temporal variation of waters emitted by MV LS has summarized in Fig. 7.

5. CONCLUSION

A total of 68 water samples from 18 mud pools of MV LS in eastern Taiwan were collected from the year 2002 to the year 2021. Their dissolved major and trace compositions as well as triple O, H, and triple Sr isotope ratios were analyzed. The results of chemical compositions and isotope ratios agree with limited previous findings (You et al. 2004; Yeh et al. 2005; Chao et al. 2011, 2013; Chang et al. 2012). Our major results are summarized as follows:

(1) The chemical composition of waters in MV LS is dominated by Cl, Na, and Ca. The high Ca/Cl, low Na/Cl, and low $^{87}Sr/^{86}Sr$ (< 0.70791) ratios relative to seawater indicate strong characteristic of water-rock interaction with igneous rock. Trace elements/Cl ratios in the MV water show similar pattern to low-temperature ridge-flank hydrothermal springs. The hybrid characteristic of sedimentary structure carrying chemically hydrothermal fluid in MV LS can be attributed to sediment-hosted geothermal system.

(2) The average values of H and triple O isotopes are slightly lower than those of seawater. The correlation of δD and $\delta^{18}O$ has a slope of 2.1, indicating MV water has similar evaporation slope to soil moisture. The δD and $\delta^{18}O$ of the water show no statistical differences among

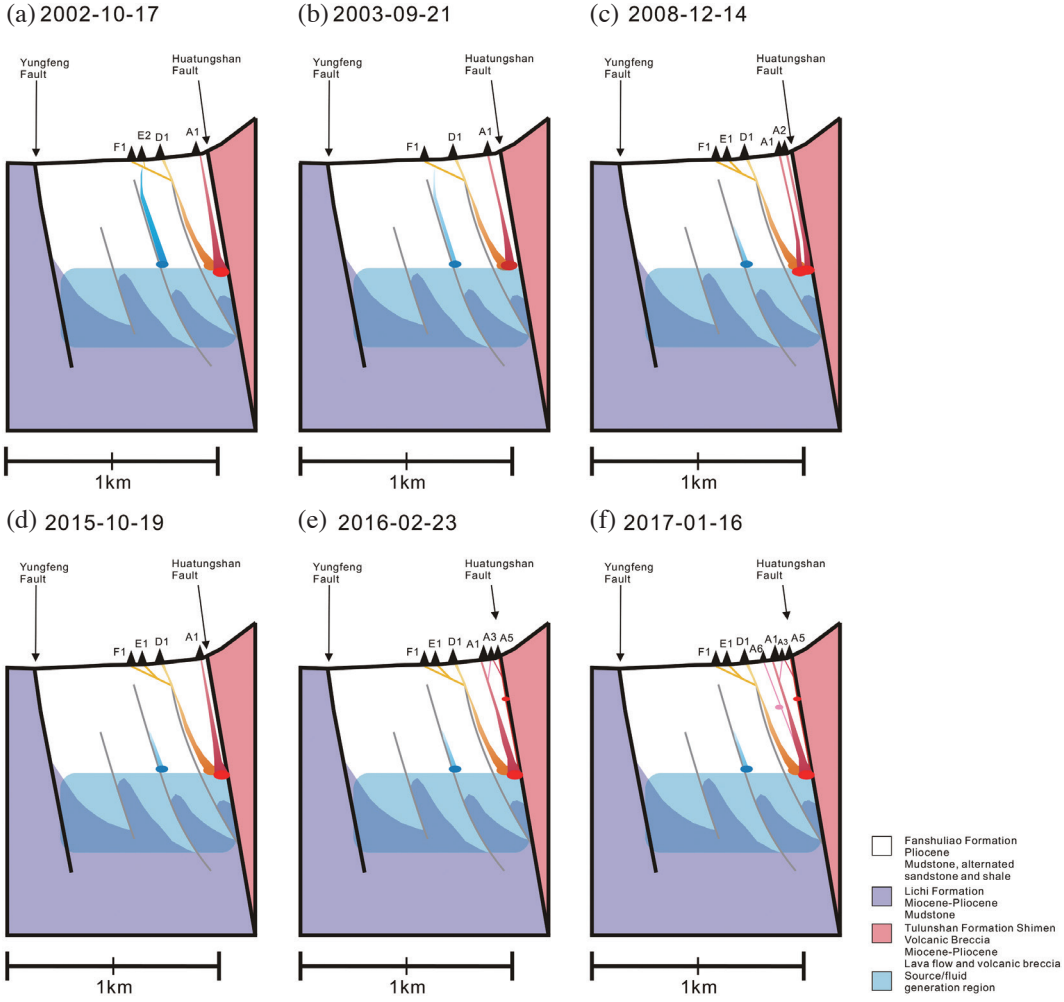

Fig. 7. A schematic diagram with E-W cross section profile shows spatial distribution of sources and reservoirs at different stage. (a) On 2002-10-17, LS-E2 and LS-F1 show sedimentary water addition. (b) On 2003-09-21, LS-E2 is dead and the sedimentary water contribution to LS-F1 decreases. LS-A1 reservoir moves slightly toward sediments. (c) On 2008-12-14, the pathway of sedimentary water from the south is closed. LS-D1, LS-E1, and LS-F1 originate from the same reservoir but different from LS-A1. LS-A1 reservoir is moving back to its previous location. (d) On 2015-10-19, LS-A1 reservoir has moved back to its previous location. (e) On 2016-02-03, LS-A5 reservoir contains less radiogenic $^{87}Sr/^{86}Sr$ water with shallower depth compared to LS-A1. LS-A3 and LS-A4 waters result from mixing of LS-A1 and LS-A5 near surface. Note that the location of LS-A1 on the figure is moved to make space for satellite mud pools. It did not move actually. (f) On 2017-01-16, LS-A6 has the same deep reservoir with LS-A1 with a shallower its own reservoir and longer residence time. Cross section profile is modified after Lo et al. (1993) and Chang et al. (2000). The horizontal scale is twice the vertical scale.

5 groups after excluding samples with low d-excess and high chloride (evaporation) as well as high d-excess and low chloride (meteoric water addition). The slight negative mass independent fractionation of oxygen isotope, $\Delta^{17}O$, may result from water-rock interaction with rocks suffering from hydrothermal alteration.

(3) The correlation of all measured components reveals 2 clusters. The first cluster is source related components: $^{87}Sr/^{86}Sr$, $\delta^{88}Sr$, Sr, K, Ge, Ba, Mo, and TA. The second cluster is evaporation varied components, which are conservative elements such as Cl^-, Br, Na, Ca, and B as well as $\delta^{18}O$, d-excess and temperature.

(4) Limited major elements, water isotopes, and small $^{87}Sr/^{86}Sr$ variation indicate the water from all mud pools of MV LS have the same source regionally. The slight increase in $^{87}Sr/^{86}Sr$ at southern groups E and F before the year 2003 may indicate the addition of sedimentary water. However, $^{87}Sr/^{86}Sr$ and Mg, K, Sr decrease down to numbers similar to those of group D after the year 2003, possibly due to the closure of sedimentary fluid channel as a consequence of the earthquake occurring in December 2003. The similar chemical and isotopic characteristic of groups D, E and F after the year 2008 may indicate the same origination of fluid reservoir and the reservoir hosts by ambient rocks with higher $^{87}Sr/^{86}Sr$ than group A's.

(5) The major mud pool at group A, LS-A1, shows small variation of source related parameters (e.g., $^{87}Sr/^{86}Sr$, Sr, K, Mg, and Rb) as well as fluid fluxes over 19 years, indicating a stable source and the location of fluid reservoir. The satellite mud pools denote mixing trend between LS-A1 and LS-A5, suggesting that LS-A5 has its own fluid reservoir.

(6) This study indicates the importance and the robustness of Sr isotopes as source and reservoir tracer for MV fluids as H and O isotopes are easily masked by evaporation and surface water addition. Waters from different reservoirs may have similar to the same H and O isotopes but different $^{87}Sr/^{86}Sr$ ratios.

Acknowledgements This study was supported by MOST grants MOST 107-2116-M-194-007, MOST 108-2116-M-194-001, MOST 109-2116-M-194-009, and MOST 110-2116-M-194-012 to HC Chao. Constructive comments by two reviewers are greatly appreciated, as well as the editors for their effective handling of this manuscript.

Authors contribution statement: HCC contributed to conception and design of the study, did the field work, performed the chemical and isotopic measurements and wrote the first draft of the manuscript. CFY, HYL, and HCL provided the instrumental resources. ITL performed the measurements of water isotopes. HCL and CHC performed analytical methods and maintain the instruments. All authors contributed to manuscript revision, read, and approved the submitted version.

Conflicts of Interest statement: Author In-Tian Lin is employed by CPC Corporation. The remaining authors declare that the research was conducted in the absence of any commercial or financial relationships that could be construed as a potential conflict of interest.

REFERENCES

Aloisi, G., M. Drews, K. Wallmann, and G. Bohrmann, 2004: Fluid expulsion from the Dvurechenskii mud volcano (Black Sea): Part I. Fluid sources and relevance to Li, B, Sr, I and dissolved inorganic nitrogen cycles. *Earth Planet. Sci. Lett.*, **225**, 347-363, doi: 10.1016/s0012-821x(04)00415-7. [Link]

Aron, P. G., N. E. Levin, E. J. Beverly, T. E. Huth, B. H. Passey, E. M. Pelletier, C. J. Poulsen, I. Z. Winkelstern, and D. A. Yarian, 2021: Triple oxygen isotopes in the water cycle. *Chem. Geol.*, **565**, 120026, doi: 10.1016/j.chemgeo.2020.120026. [Link]

Bentahila, Y., D. B. Othman, and J.-M. Luck, 2008: Strontium, lead and zinc isotopes in marine cores as tracers of sedimentary provenance: A case study around Taiwan orogen. *Chem. Geol.*, **248**, 62-82, doi: 10.1016/j.chemgeo.2007.10.024. [Link]

Bonini, M., 2021: Structural controls and earthquake response of Taiwan mud volcanoes. *Mar. Pet. Geol.*, **128**, 105050, doi: 10.1016/j.marpetgeo.2021.105050. [Link]

Bonini, M., M. L. Rudolph, and M. Manga, 2016: Long- and short-term triggering and modulation of mud volcano eruptions by earthquakes. *Tectonophysics*, **672-673**, 190-211, doi: 10.1016/j.tecto.2016.01.037. [Link]

Bray, C. J. and D. E. Karig, 1985: Porosity of sediments in accretionary prisms and some implications for dewatering processes. *J. Geophys. Res.*, **90**, 768-778, doi: 10.1029/JB090iB01p00768. [Link]

Chang, C.-P., J. Angelier, and C.-Y. Huang, 2000: Origin and evolution of a mélange: The active plate boundary and suture zone of the Longitudinal Valley, Taiwan. *Tectonophysics*, **325**, 43-62, doi: 10.1016/S0040-1951(00)00130-X. [Link]

Chang, Y.-H., T.-W. Cheng, W.-J. Lai, W.-Y. Tsai, C.-H. Sun, L.-H. Lin, and P.-L. Wang, 2012: Microbial methane cycling in a terrestrial mud volcano in eastern Taiwan. *Environ. Microbiol.*, **14**, 895-908, doi: 10.1111/j.1462-2920.2011.02658.x. [Link]

Chao, H.-C., C.-F. You, and C.-H. Sun, 2010: Gases in Taiwan mud volcanoes: Chemical composition, methane carbon isotopes, and gas fluxes. *Appl. Geochem.*, **25**, 428-436, doi: 10.1016/j.apgeochem.2009.12.009. [Link]

Chao, H.-C., C.-F. You, B.-S. Wang, C.-H. Chung, and K.-F. Huang, 2011: Boron isotopic composition of mud volcano fluids: Implications for fluid migration in shallow

subduction zones. *Earth Planet. Sci. Lett.*, **305**, 32-44, doi: 10.1016/j.epsl.2011.02.033. [Link]

Chao, H.-C., C.-F. You, H.-C. Liu, and C.-H. Chung, 2013: The origin and migration of mud volcano fluids in Taiwan: Evidence from hydrogen, oxygen, and strontium isotopic compositions. *Geochim. Cosmochim. Acta*, **114**, 29-51, doi: 10.1016/j.gca.2013.03.035. [Link]

Chao, H.-C., C.-F. You, H.-C. Liu, and C.-H. Chung, 2015: Evidence for stable Sr isotope fractionation by silicate weathering in a small sedimentary watershed in southwestern Taiwan. *Geochim. Cosmochim. Acta*, **165**, 324-341, doi: 10.1016/j.gca.2015.06.006. [Link]

Chao, H.-C., C.-F. You, I.-T. Lin, H.-C. Liu, L.-H. Chung, C.-C. Huang, and C.-H. Chung, 2022: Two-end-member mixing in the fluids emitted from Mud Volcano Lei-Gong-Huo, Eastern Taiwan: Evidence from Sr isotopes. *Front. Earth Sci.*, **9**, 750436, doi: 10.3389/feart.2021.750436. [Link]

Chen, C.-H., Y.-N. Shieh, T. Lee, C.-H. Chen, and S. A. Mertzman, 1990: Nd-Sr-O isotopic evidence for source contamination and an unusual mantle component under Luzon Arc. *Geochim. Cosmochim. Acta*, **54**, 2473-2483, doi: 10.1016/0016-7037(90)90234-C. [Link]

Chen, N.-C., T. F. Yang, W.-L. Hong, T.-L. Yu, I.-T. Lin, P.-L. Wang, S. Lin, C.-C. Su, C.-C. Shen, Y. Wang, and L.-H. Lin, 2020: Discharge of deeply rooted fluids from submarine mud volcanism in the Taiwan accretionary prism. *Sci. Rep.*, **10**, 381, doi: 10.1038/s41598-019-57250-9. [Link]

Ching, K.-E., R.-J. Rau, and Y. Zeng, 2007: Coseismic source model of the 2003 M_w 6.8 Chengkung earthquake, Taiwan, determined from GPS measurements. *J. Geophys. Res.*, **112**, B06422, doi: 10.1029/2006JB004439. [Link]

Ching, K.-E., R.-J. Rau, K. M. Johnson, J.-C. Lee, and J.-C. Hu, 2011: Present-day kinematics of active mountain building in Taiwan from GPS observations during 1995–2005. *J. Geophys. Res.*, **116**, B09405, doi: 10.1029/2010JB008058. [Link]

Chung, C.-H., C.-F. You, and H.-Y. Chu, 2009: Weathering sources in the Gaoping (Kaoping) river catchments, southwestern Taiwan: Insights from major elements, Sr isotopes, and rare earth elements. *J. Mar. Syst.*, **76**, 433-443, doi: 10.1016/j.jmarsys.2007.09.013. [Link]

Dahlmann, A. and G. J. de Lange, 2003: Fluid–sediment interactions at Eastern Mediterranean mud volcanoes: A stable isotope study from ODP Leg 160. *Earth Planet. Sci. Lett.*, **212**, 377-391, doi: 10.1016/S0012-821X(03)00227-9. [Link]

Delisle, G., U. von Rad, H. Andruleit, C. von Daniels, A. Tabrez, and A. Inam, 2002: Active mud volcanoes on- and offshore eastern Makran, Pakistan. *Int. J. Earth Sci.*, **91**, 93-110, doi: 10.1007/s005310100203. [Link]

Deville, E. and S.-H. Guerlais, 2009: Cyclic activity of mud volcanoes: Evidences from Trinidad (SE Caribbean). *Mar. Pet. Geol.*, **26**, 1681-1691, doi: 10.1016/j.marpetgeo.2009.03.002. [Link]

Dia, A. N., M. Castrec, J. Boulègue, and J. P. Boudou, 1995: Major and trace element and Sr isotope constraints on fluid circulations in the Barbados accretionary complex. Part 1: Fluid origin. *Earth Planet. Sci. Lett.*, **134**, 69-85, doi: 10.1016/0012-821X(95)00102-I. [Link]

Dia, A. N., M. Castrec-Rouelle, J. Boulègue, and P. Comeau, 1999: Trinidad mud volcanoes: Where do the expelled fluids come from? *Geochim. Cosmochim. Acta*, **63**, 1023-1038, doi: 10.1016/S0016-7037(98)00309-3. [Link]

Dimitrov, L. I., 2002: Mud volcanoes—The most important pathway for degassing deeply buried sediments. *Earth-Sci. Rev.*, **59**, 49-76, doi: 10.1016/S0012-8252(02)00069-7. [Link]

Dincer, T., A. Al-Mugrin, and U. Zimmermann, 1974: Study of the infiltration and recharge through the sand dunes in arid zones with special reference to the stable isotopes and thermonuclear tritium. *J. Hydrol.*, **23**, 79-109, doi: 10.1016/0022-1694(74)90025-0. [Link]

Etiope, G., A. Caracausi, R. Favara, F. Italiano, and C. Baciu, 2002: Methane emission from the mud volcanoes of Sicily (Italy). *Geophys. Res. Lett.*, **29**, 56-1-56-4, doi: 10.1029/2001GL014340. [Link]

Etiope, G., G. Martinelli, A. Caracausi, and F. Italiano, 2007: Methane seeps and mud volcanoes in Italy: Gas origin, fractionation and emission to the atmosphere. *Geophys. Res. Lett.*, **34**, doi: 10.1029/2007GL030341. [Link]

Etiope, G., A. Feyzullayev, and C. L. Baciu, 2009: Terrestrial methane seeps and mud volcanoes: A global perspective of gas origin. *Mar. Pet. Geol.*, **26**, 333-344, doi: 10.1016/j.marpetgeo.2008.03.001. [Link]

Etiope, G., C. L. Baciu, and M. Schoell, 2011a: Extreme methane deuterium, nitrogen and helium enrichment in natural gas from the Homorod seep (Romania). *Chem. Geol.*, **280**, 89-96, doi: 10.1016/j.chemgeo.2010.10.019. [Link]

Etiope, G., R. Nakada, K. Tanaka, and N. Yoshida, 2011b: Gas seepage from Tokamachi mud volcanoes, onshore Niigata Basin (Japan): Origin, post-genetic alterations and CH_4–CO_2 fluxes. *Appl. Geochem.*, **26**, 348-359, doi: 10.1016/j.apgeochem.2010.12.008. [Link]

Farhadian Babadi, M., B. Mehrabi, F. Tassi, J. Cabassi, O. Vaselli, A. Shakeri, E. Pecchioni, S. Venturi, M. Zelenski, and I. Chaplygin, 2019: Origin of fluids discharged from mud volcanoes in SE Iran. *Mar. Pet. Geol.*, **106**, 190-205, doi: 10.1016/j.marpetgeo.2019.05.005. [Link]

Garlick, G. D. and J. R. Dymond, 1970: Oxygen isotope exchange between volcanic materials and ocean water. *Geol. Soc. Am. Bull.*, **81**, 2137-2142, doi:

10.1130/0016-7606(1970)81[2137:OIEBVM]2.0.CO;2. [Link]

Gieskes, J. M., M. Kastner, and T. B. Warner, 1975: Evidence for extensive diagenesis, Madagascar Basin, Deep Sea Drilling Site 245. *Geochim. Cosmochim. Acta*, **39**, 1385-1393, doi: 10.1016/0016-7037(75)90117-9. [Link]

Gieskes, J. M., P. Vrolijk, and G. Blanc, 1990: Hydrogeochemistry of the Northern Barbados Accretionary Complex Transect: Ocean Drilling Project Leg 110. *J. Geophys. Res.*, **95**, 8809-8818, doi: 10.1029/JB095iB06p08809. [Link]

Giggenbach, W. F., 1988: Geothermal solute equilibria. Derivation of Na-K-Mg-Ca geoindicators. *Geochim. Cosmochim. Acta*, **52**, 2749-2765, doi: 10.1016/0016-7037(88)90143-3. [Link]

Halicz, L., I. Segal, N. Fruchter, M. Stein, and B. Lazar, 2008: Strontium stable isotopes fractionate in the soil environments? *Earth Planet. Sci. Lett.*, **272**, 406-411, doi: 10.1016/j.epsl.2008.05.005. [Link]

Henderson, P., 1982: Inorganic Geochemistry, Pergamon Press, New York, 343 pp.

Hensen, C., K. Wallmann, M. Schmidt, C. R. Ranero, and E. Suess, 2004: Fluid expulsion related to mud extrusion off Costa Rica—A window to the subducting slab. *Geology*, **32**, 201-204, doi: 10.1130/G20119.1. [Link]

Huang, K.-F., C.-F. You, C.-H. Chung, and I.-T. Lin, 2011: Nonhomogeneous seawater Sr isotopic composition in the coastal oceans: A novel tool for tracing water masses and submarine groundwater discharge. *Geochem. Geophys. Geosyst.*, **12**, Q05002, doi: 10.1029/2010GC003372. [Link]

Jiang, G.-J., J. Angelier, J.-C. Lee, H.-T. Chu, J.-C. Hu, and C.-H. Mu, 2011: Faulting and Mud Volcano Eruptions Inside of the Coastal Range During the 2003 M_w = 6.8 Chengkung Earthquake in Eastern Taiwan. *Terr. Atmos. Ocean. Sci.*, **22**, 463-473, doi: 10.3319/TAO.2011.04.22.01(TT). [Link]

Kopf, A. J., 2002: Significance of mud volcanism. *Rev. Geophys.*, **40**, 2-1-2-52, doi: 10.1029/2000RG000093. [Link]

Kopf, A. J. and A. Deyhle, 2002: Back to the roots: Boron geochemistry of mud volcanoes and its implications for mobilization depth and global B cycling. *Chem. Geol.*, **192**, 195-210, doi: 10.1016/S0009-2541(02)00221-8. [Link]

Krabbenhöft, A., J. Fietzke, A. Eisenhauer, V. Liebetrau, F. Böhm, and H. Vollstaedt, 2009: Determination of radiogenic and stable strontium isotope ratios ($^{87}Sr/^{86}Sr$; $\delta^{88/86}Sr$) by thermal ionization mass spectrometry applying an $^{87}Sr/^{84}Sr$ double spike. *J. Anal. At. Spectrom.*, **24**, 1267-1271, doi: 10.1039/B906292K. [Link]

Land, M., J. Ingri, P. S. Andersson, and B. Öhlander, 2000: Ba/Sr, Ca/Sr and $^{87}Sr/^{86}Sr$ ratios in soil water and groundwater: Implications for relative contributions to stream water discharge. *Appl. Geochem.*, **15**, 311-325, doi: 10.1016/S0883-2927(99)00054-2. [Link]

Lavrushin, V. Y., A. Kopf, A. Deyhle, and M. I. Stepanets, 2003: Formation of Mud-Volcanic Fluids in Taman (Russia) and Kakhetia (Georgia): Evidence from Boron Isotopes. *Lithol. Miner. Resour.*, **38**, 120-153, doi: 10.1023/A:1023452025440. [Link]

Lavrushin, V. Y., E. O. Dubinina, and A. S. Avdeenko, 2005: Isotopic composition of oxygen and hydrogen in mud-volcanic waters from Taman (Russia) and Kakhetia (Eastern Georgia). *Lithol. Miner. Resour.*, **40**, 123-137, doi: 10.1007/s10987-005-0014-z. [Link]

Lavrushin, V. Y., I. S. Guliev, O. E. Kikvadze, A. A. Aliev, B. G. Pokrovsky, and B. G. Polyak, 2015: Waters from mud volcanoes of Azerbaijan: Isotopic-geochemical properties and generation environments. *Lithol. Miner. Resour.*, **50**, 1-25, doi: 10.1134/S0024490215010034. [Link]

Lawrence, J. R. and J. M. Gieskes, 1981: Constraints on water transport and alteration in the oceanic crust from the isotopic composition of pore water. *J. Geophys. Res.*, **86**, 7924-7934, doi: 10.1029/JB086iB09p07924. [Link]

Li, Y.-H., 1976: Denudation of Taiwan island since the Pliocene epoch. *Geology*, **4**, 105-107, doi: 10.1130/0091-7613(1976)4<105:DOTIST>2.0.CO;2. [Link]

Lin, C.-T., R. Harris, W.-D. Sun, and G.-L. Zhang, 2019: Geochemical and geochronological constraints on the origin and emplacement of the East Taiwan ophiolite. *Geochem. Geophys. Geosyst.*, **20**, 2110-2133, doi: 10.1029/2018GC007902. [Link]

Lin, K.-C., J.-C. Hu, K.-E. Ching, J. Angelier, R.-J. Rau, S.-B. Yu, C.-H. Tsai, T.-C. Shin, and M.-H. Huang, 2010: GPS crustal deformation, strain rate, and seismic activity after the 1999 Chi-Chi earthquake in Taiwan. *J. Geophys. Res.*, **115**, B07404, doi: 10.1029/2009JB006417. [Link]

Liu, H.-C., C.-F. You, K.-F. Huang, and C.-H. Chung, 2012: Precise determination of triple Sr isotopes ($\delta^{87}Sr$ and $\delta^{88}Sr$) using MC-ICP-MS. *Talanta*, **88**, 338-344, doi: 10.1016/j.talanta.2011.10.050. [Link]

Lo, H. J., W. S. Chen, and S. R. Song, 1993: Explanatory Text of the Geologic Map of Taiwan: Chengkung and Tungho, Sheets 54, 60, Scale 1:50,000, Central Geological Survey, MOEA, Taipei, Taiwan.

Mazzini, A. and G. Etiope, 2017: Mud volcanism: An updated review. *Earth-Sci. Rev.*, **168**, 81-112, doi: 10.1016/j.earscirev.2017.03.001. [Link]

Mazzini, A., H. Svensen, G. G. Akhmanov, G. Aloisi, S. Planke, A. Malthe-Sørenssen, and B. Istadi, 2007: Triggering and dynamic evolution of the LUSI mud volcano, Indonesia. *Earth Planet. Sci. Lett.*, **261**, 375-388, doi: 10.1016/j.epsl.2007.07.001. [Link]

Mazzini, A., H. Svensen, S. Planke, I. Guliyev, G. G. Akhmanov, T. Fallik, and D. Banks, 2009: When mud volcanoes sleep: Insight from seep geochemistry at the Dashgil mud volcano, Azerbaijan. *Mar. Pet. Geol.*, **26**, 1704-1715, doi: 10.1016/j.marpetgeo.2008.11.003. [Link]

Mazzini, A., F. Scholz, H. H. Svensen, C. Hensen, and S. Hadi, 2018: The geochemistry and origin of the hydrothermal water erupted at Lusi, Indonesia. *Mar. Pet. Geol.*, **90**, 52-66, doi: 10.1016/j.marpetgeo.2017.06.018. [Link]

Milkov, A. V., 2000: Worldwide distribution of submarine mud volcanoes and associated gas hydrates. *Mar. Geol.*, **167**, 29-42, doi: 10.1016/S0025-3227(00)00022-0. [Link]

Millero, F. J., R. Feistel, D. G. Wright, and T. J. McDougall, 2008: The composition of Standard Seawater and the definition of the Reference-Composition Salinity Scale. *Deep-Sea Res. Part I-Oceanogr. Res. Pap.*, **55**, 50-72, doi: 10.1016/j.dsr.2007.10.001. [Link]

Paytan, A., E. M. Griffith, A. Eisenhauer, M. P. Hain, K. Wallmann, and A. Ridgwell, 2021: A 35-million-year record of seawater stable Sr isotopes reveals a fluctuating global carbon cycle. *Science*, **371**, 1346-1350, doi: 10.1126/science.aaz9266. [Link]

Peng, T.-R., C.-H. Wang, C.-C. Huang, L.-Y. Fei, C.-T. A. Chen, and J.-L. Hwong, 2010: Stable isotopic characteristic of Taiwan's precipitation: A case study of western Pacific monsoon region. *Earth Planet. Sci. Lett.*, **289**, 357-366, doi: 10.1016/j.epsl.2009.11.024. [Link]

Perry, E. A., J. M. Gieskes, and J. R. Lawrence, 1976: Mg, Ca and O^{18}/O^{16} exchange in the sediment-pore water system, hole 149, DSDP. *Geochim. Cosmochim. Acta*, **40**, 413-423, doi: 10.1016/0016-7037(76)90006-5. [Link]

Planke, S., H. Svensen, M. Hovland, D. A. Banks, and B. Jamtveit, 2003: Mud and fluid migration in active mud volcanoes in Azerbaijan. *Geo-Mar. Lett.*, **23**, 258-268, doi: 10.1007/s00367-003-0152-z. [Link]

Procesi, M., G. Ciotoli, A. Mazzini, and G. Etiope, 2019: Sediment-hosted geothermal systems: Review and first global mapping. *Earth-Sci. Rev.*, **192**, 529-544, doi: 10.1016/j.earscirev.2019.03.020. [Link]

Ray, J. S., A. Kumar, A. K. Sudheer, R. D. Deshpande, D. K. Rao, D. J. Patil, N. Awasthi, R. Bhutani, R. Bhushan, and A. M. Dayal, 2013: Origin of gases and water in mud volcanoes of Andaman accretionary prism: Implications for fluid migration in forearcs. *Chem. Geol.*, **347**, 102-113, doi: 10.1016/j.chemgeo.2013.03.015. [Link]

Sengupta, S. and A. Pack, 2018: Triple oxygen isotope mass balance for the Earth's oceans with application to Archean cherts. *Chem. Geol.*, **495**, 18-26, doi: 10.1016/j.chemgeo.2018.07.012. [Link]

Sengupta, S., S. T. M. Peters, J. Reitner, J.-P. Duda, and A. Pack, 2020: Triple oxygen isotopes of cherts through time. *Chem. Geol.*, **554**, 119789, doi: 10.1016/j.chemgeo.2020.119789. [Link]

Seyfried, W. E. and J. L. Bischoff, 1979: Low temperature basalt alteration by sea water: An experimental study at 70°C and 150°C. *Geochim. Cosmochim. Acta*, **43**, 1937-1947, doi: 10.1016/0016-7037(79)90006-1. [Link]

Shakirov, R., A. Obzhirov, E. Suess, A. Salyuk, and N. Biebow, 2004: Mud volcanoes and gas vents in the Okhotsk Sea area. *Geo-Mar. Lett.*, **24**, 140-149, doi: 10.1007/s00367-004-0177-y. [Link]

Sharp, Z. D., J. A. G. Wostbrock, and A. Pack, 2018: Mass-dependent triple oxygen isotope variations in terrestrial materials. *Geochem. Perspect. Lett.*, **7**, 27-31, doi: 10.7185/geochemlet.1815. [Link]

Shih, T.-T., 1967: A survey of the active mud volcanoes in Taiwan and a study of their types and the character of the mud. *Petrol. Geol. Taiwan*, **5**, 259-311.

Sun, C.-H., S.-C. Chang, C.-L. Kuo, J.-C. Wu, P.-H. Shao, and J.-N. Oung, 2010: Origins of Taiwan's mud volcanoes: Evidence from geochemistry. *J. Asian Earth Sci.*, **37**, 105-116, doi: 10.1016/j.jseaes.2009.02.007. [Link]

Teng, L. S., 1990: Geotectonic evolution of late Cenozoic arc-continent collision in Taiwan. *Tectonophysics*, **183**, 57-76, doi: 10.1016/0040-1951(90)90188-E. [Link]

Ullman, W. J. and R. C. Aller, 1983: Rates of iodine remineralization in terrigenous near-shore sediments. *Geochim. Cosmochim. Acta*, **47**, 1423-1432, doi: 10.1016/0016-7037(83)90301-0. [Link]

Verma, S. P., K. Pandarinath, and E. Santoyo, 2008: SolGeo: A new computer program for solute geothermometers and its application to Mexican geothermal fields. *Geothermics*, **37**, 597-621, doi: 10.1016/j.geothermics.2008.07.004. [Link]

Wheat, C. G. and M. J. Mottl, 2000: Composition of pore and spring waters from Baby Bare: Global implications of geochemical fluxes from a ridge flank hydrothermal system. *Geochim. Cosmochim. Acta*, **64**, 629-642, doi: 10.1016/S0016-7037(99)00347-6. [Link]

Wheat, C. G., M. J. Mottl, and M. Rudnicki, 2002: Trace element and REE composition of a low-temperature ridge-flank hydrothermal spring. *Geochim. Cosmochim. Acta*, **66**, 3693-3705, doi: 10.1016/S0016-7037(02)00894-3. [Link]

Yang, T. F., C.-H. Chen, R. L. Tien, S. R. Song, and T. K. Liu, 2003: Remnant magmatic activity in the Coastal Range of east Taiwan after arc–continent collision: Fission-track data and $^{3}He/^{4}He$ ratio evidence. *Radiat. Meas.*, **36**, 343-349, doi: 10.1016/S1350-4487(03)00149-5. [Link]

Yang, T. F., G.-H. Yeh, C.-C. Fu, C.-C. Wang, T.-F. Lan, H.-F. Lee, C.-H. Chen, V. Walia, and Q.-C. Sung,

2004: Composition and exhalation flux of gases from mud volcanoes in Taiwan. *Environ. Geol.*, **46**, 1003-1011, doi: 10.1007/s00254-004-1086-0. [Link]

Yeh, G.-H., T. F. Yang, J.-C. Chen, Y.-G. Chen, and S.-R. Song, 2005: Fluid geochemistry of mud volcanoes in Taiwan. In: Martinelli, G. and B. Panahi (Eds.), Mud Volcanoes, Geodynamics and Seismicity, NATO Science Series, Vol. 51, Springer, Dordrecht, 227-237, doi: 10.1007/1-4020-3204-8_21. [Link]

You, C.-F., A. J. Spivack, J. H. Smith, and J. M. Gieskes, 1993: Mobilization of boron in convergent margins: Implications for the boron geochemical cycle. *Geology*, **21**, 207-210, doi: 10.1130/0091-7613(1993)021<0207:MOBICM>2.3.CO;2. [Link]

You, C.-F., P. R. Castillo, J. M. Gieskes, L. H. Chan, and A. J. Spivack, 1996: Trace element behavior in hydrothermal experiments: Implications for fluid processes at shallow depths in subduction zones. *Earth Planet. Sci. Lett.*, **140**, 41-52, doi: 10.1016/0012-821X(96)00049-0. [Link]

You, C.-F., J. M. Gieskes, T. Lee, T.-F. Yui, and H.-W. Chen, 2004: Geochemistry of mud volcano fluids in the Taiwan accretionary prism. *Appl. Geochem.*, **19**, 695-707, doi: 10.1016/j.apgeochem.2003.10.004. [Link]

Yu, S.-B., H.-Y. Chen, and L.-C. Kuo, 1997: Velocity field of GPS stations in the Taiwan area. *Tectonophysics*, **274**, 41-59, doi: 10.1016/S0040-1951(96)00297-1. [Link]

APPENDIX A.

Table A1. Dissolved components over chloride ratios of MV LS waters.

	Na/Cl $\times 10^{-3}$	Ca/Cl $\times 10^{-3}$	Mg/Cl $\times 10^{-3}$	B/Cl $\times 10^{-3}$	TA/Cl $\times 10^{-3}$	K/Cl $\times 10^{-3}$	Br/Cl $\times 10^{-3}$	Si/Cl $\times 10^{-6}$	Sr/Cl $\times 10^{-6}$	S/Cl $\times 10^{-6}$	Ba/Cl $\times 10^{-6}$	Mn/Cl $\times 10^{-6}$	Fe/Cl $\times 10^{-6}$	I/Cl $\times 10^{-6}$	Li/Cl $\times 10^{-6}$
LS-A1_2002	576	220	1.94	4.87		1.79	1.29	741	325	182	30.4	148	0.23	65.7	56.5
LS-A1_2003a	569	218	3.26	4.63		1.84	1.31	526	333	195	25.1	8.9	0.10	4.10	41.4
LS-A1_2003b	564	214	3.15	4.56		1.97	1.35	438	329	191	25.6	13.8	0.00	5.88	40.4
LS-A1_2003c	563	215	3.03	4.55		1.88	1.36	475	327	187	25.5	23.6	1.35	6.74	40.4
LS-A1_2008[a]	537	207	2.03	3.93		2.32	1.25	467	313	86.9	17.6	112	0.13	50.1	48.5
LS-A1_2015-1[b]	574	219	1.20	4.72	3.48	1.58	1.35	708	311	172	22.7	32.6	0.18	58.8	55.8
LS-A1_2015-2[b]	579	223	1.15	4.78	2.97	1.56	1.37	1000	316	174	22.6	34.2	0.00	59.5	56.2
LS-A1_2016-1[b]	568	231	1.18	4.79	2.43	1.64	1.42	897	327	175	25.8	69.6	0.47	63.0	57.3
LS-A1_2016-2[b]	548	219	1.17	4.57	2.19	1.47	1.34	759	314	165	24.2	63.7	0.32	14.1	55.2
LS-A1_2016-3[b]	539	214	1.13	4.52	2.31	1.43	1.32	857	308	165	23.6	61.2	0.41	30.4	53.5
LS-A1_2016-4[b]	561	220	1.25	4.58	1.77	1.58	1.44	736	321	172	23.4	60.3	0.04	63.3	56.0
LS-A1_2016-5[b]	538	212	1.15	4.44	3.03	1.41	1.35	758	307	169	23.7	58.0	0.08	52.5	54.1
LS-A1_2016-6[b]	555	217	1.18	4.54	2.77	1.50	1.39	811	310	170	24.4	52.5	0.00	52.0	56.2
LS-A1_2016-7[b]	554	217	1.16	4.59	2.81	1.60	1.39	802	312	172	25.0	56.2	0.07	32.3	56.2
LS-A1_2017[b]	560	219	1.31	4.59	2.78	1.89	1.39	697	324	171	24.4	66.0	0.00	35.3	52.9
LS-A1_2018	528	212	1.08	4.10	1.51	1.51	1.53	413	301	168	22.4	31.1	0.23	43.9	50.9
LS-A1_2019	552	217	1.15	4.51	1.84	1.56	1.53	665	315	163	25.3	55.9	0.00	31.7	54.5
LS-A1_2020	568	218	1.15	4.56	2.26	1.60	1.49	799	317	252	24.0	46.8	0.17	11.6	58.1
LS-A1_2021	568	217	0.962	4.57	1.89	1.63	1.49	657	312	247	22.5	43.5	0.00	23.0	57.4
LS-A2_2008[a]	541	212	1.61	4.00		2.18	1.26	482	305	106	21.9	120	0.07	53.1	58.9
LS-A3_2015-2	601	224	3.50	4.86	4.16	0.942	1.37	1160	278	176	15.1	219	136	45.8	6.84
LS-A3_2016-2	550	217	4.36	4.57	4.09	0.965	1.35	1370	253	161	6.79	148	0.13	45.7	4.61
LS-A3_2016-3	525	210	3.40	4.25	5.32	1.07	1.34	498	269	182	14.4	141	0.57	42.8	16.7
LS-A3_2016-5	543	208	3.69	4.32	5.07	0.835	1.37	445	260	163	16.1	193	1.99	48.9	5.50
LS-A3_2016-6	559	210	3.60	4.42	4.52	0.878	1.34	717	259	167	16.6	219	28	46.1	4.78
LS-A3_2016-7	556	215	1.63	4.60	2.84	1.44	1.35	604	303	181	22.5	77.0	0.10	36.0	46.7
LS-A3_2017	563	213	3.57	4.47	4.59	1.11	1.43	674	268	168	18.9	183	98.5	44.3	4.28
LS-A4_2016-1	574	226	3.92	4.61	4.37	0.907	1.42	624	281	178	17.8	251	0.28	52.3	9.12
LS-A4_2016-3	530	203	4.23	4.27	4.03	1.03	1.32	1100	244	159	6.72	118	0.11	44.8	5.34
LS-A4_2016-5	547	209	4.29	4.37	6.29	1.01	1.41	998	254	165	7.43	183	24.3	66.2	4.87
LS-A4_2016-6	565	212	4.29	4.43	5.45	1.07	1.35	1130	254	163	7.25	173	10.6	36.6	4.02
LS-A4_2016-7	572	213	4.25	4.59	4.52	1.17	1.39	1050	258	166	9.16	136	0.76	46.6	5.50

Note: a: Data adopted from Chao et al. (2011). b: Data adopted from Chao et al. (2022).

Table A1. (Continued)

	Na/Cl × 10^{-3}	Ca/Cl × 10^{-3}	Mg/Cl × 10^{-3}	B/Cl × 10^{-3}	TA/Cl × 10^{-3}	K/Cl × 10^{-3}	Br/Cl × 10^{-3}	Si/Cl × 10^{-6}	Sr/Cl × 10^{-6}	S/Cl × 10^{-6}	Ba/Cl × 10^{-6}	Mn/Cl × 10^{-6}	Fe/Cl × 10^{-6}	I/Cl × 10^{-6}	Li/Cl × 10^{-6}
LS-A4_2017	566	213	4.38	4.54	5.29	1.39	1.41	1570	256	165	6.67	140	0.00	37.3	4.47
LS-A4_2018	536	206	4.02	4.29	3.91	1.30	1.40	1390	259	160	5.24	155	0.12	39.2	5.56
LS-A4_2019	569	215	4.37	4.57	4.46	1.25	1.48	1510	268	162	5.58	162	0.00	43.4	5.37
LS-A4_2020	567	210	4.24	4.51	3.94	1.22	1.49	1370	259	241	5.39	139	0.36	21.9	6.03
LS-A5_2016-2	548	216	5.32	4.33	4.46	0.652	1.34	1080	215	162	11.7	209	14.6	51.0	1.63
LS-A5_2016-3	532	206	5.10	4.14	3.92	0.617	1.35	1090	210	158	9.62	208	1.03	59.1	1.54
LS-A5_2017	565	214	5.32	4.43	4.65	0.977	1.42	1010	220	167	12.1	201	80.1	35.3	1.71
LS-A6_2017	552	217	2.39	4.46	5.58	1.58	1.43	597	310	171	14.7	212	0.33	35.8	25.2
LS-A6_2018	517	210	2.86	4.06	4.97	1.52	1.42	508	295	169	15.5	319	0.35	47.3	19.1
LS-A6_2019	557	223	4.56	4.37	6.22	1.66	1.51	505	319	206	16.5	317	89.3	60.0	15.8
LS-B1_2002	572	221	1.21	4.60		1.49	1.36	858	341	181	119	0.07	0.23	12.6	57.5
LS-B2_2021	562	209	2.74	4.45	3.42	1.43	1.50	1110	306	237	12.4	96.8	0.09	21.5	23.0
LS-D1_2002	574	223	2.08	4.96		1.97	1.35	386	356	418	25.7	0.56	0.59	2.11	42.0
LS-D1_2003	552	212	2.00	4.74		1.69	1.36	1690	347	188	94.2	1.85	1.80	22.8	60.5
LS-D1_2008[a]	541	210	2.67	4.14		2.45	1.27	579	351	191	80.4	48.1	0.59	102.0	64.7
LS-D1_2017	568	219	1.66	4.70	2.87	1.87	1.46	1060	365	171	107	27.2	0.00	39.8	60.4
LS-D1_2018	533	209	1.62	4.30	2.16	1.78	1.41	746	343	166	109	16.0	0.05	52.3	57.2
LS-D1_2019	527	202	1.71	4.36	2.02	1.57	1.38	1070	342	153	101	23.2	0.00	34.6	55.2
LS-D1_2020	563	213	1.56	4.62	1.86	1.79	1.47	1160	359	248	111	17.1	0.15	10.3	63.9
LS-D1_2021	570	212	1.45	4.51	2.16	1.70	1.50	1040	357	242	103	14.9	0.01	32.1	58.4
LS-D2_2008[a]	544	209	2.13	4.29		2.50	1.27	1110	388	101	76.7	37.5	0.23	83.6	74.5
LS-D3_2002	557	213	1.47	5.03		1.83	1.31	386	328	214	82.6	0.12	0.00	5.70	43.4
LS-E1_2008[a]	535	206	1.10	4.42		2.38	1.25	1080	374	105	39.8	39.1	0.34	24.8	76.7
LS-E1_2017	573	221	1.59	5.01	3.05	1.87	1.44	1310	402	172	51.6	38.0	0.00	31.2	67.7
LS-E1_2018	535	210	1.58	4.72	2.14	1.74	1.42	1080	376	168	48.8	38.6	0.13	46.0	65.6
LS-E1_2019	536	205	1.41	4.68	1.94	1.59	1.40	1200	374	153	45.4	34.6	0.00	29.3	62.9
LS-E1_2020	572	215	1.51	4.95	2.41	1.75	1.50	1370	395	251	47.8	34.5	0.13	17.5	69.5
LS-E1_2021	566	211	1.25	4.76	2.16	1.68	1.45	1300	384	237	41.5	32.2	0.08	24.4	63.8
LS-E2_2002	563	198	7.14	5.00		2.54	1.29	353	615	398	35.7	12.6	0.93	18.0	56.7
LS-E3_2017	572	222	1.09	5.08	2.08	1.93	1.48	1260	388	175	45.7	25.8	0.00	55.5	68.0
LS-E4_2021	566	190	3.96	4.63	2.20	1.80	1.42	1070	491	217	124	38.7	0.01	23.6	66.4
LS-F1_2002	550	194	13.2	4.47		2.90	1.27	519	810	197	123	0.24	0.94	9.28	70.9
LS-F1_2003	545	194	12.5	4.84		2.63	1.27	782	673	181	508	10.4	0.32	6.34	71.0
LS-F1_2008[a]	532	203	1.31	4.34		2.33	1.20	1150	376	90.4	62.4	16.4	0.03	49.4	75.4
LS-F2_2008[a]	556	211	1.38	4.50		2.41	1.27	1390	386	131	39.5	27.4	0.09	66.6	79.6
LS-F3_2008[a]	550	208	0.801	4.48		2.39	1.26	1340	380	138	29.0	5.82	0.92	68.5	80.6
Seawater	859	18.8	96.8	0.761	4.27	18.7	1.54	189	166	51700	0.080	0.01	0.11	0.92	49.9
minimum	517	190	0.801	3.93	1.51	0.617	1.20	353	210	86.9	5.24	0.07	0.00	2.11	1.54
maximum	601	231	13.2	5.08	6.29	2.90	1.53	1690	810	418	508	319	136	102.0	80.6
average	555	213	2.83	4.54	3.41	1.61	1.38	892	334	183	44.4	87.9	7.43	38.3	42.1
SD	16	8	2.28	0.25	1.32	0.49	0.08	334	96	53	66.6	81.2	24.8	20.2	25.4

Table A1. (Continued)

	Al/Cl × 10^{-6}	Ti/Cl × 10^{-9}	Co/Cl × 10^{-9}	Ni/Cl × 10^{-9}	Cu/Cl × 10^{-9}	Zn/Cl × 10^{-9}	Ge/Cl × 10^{-9}	As/Cl × 10^{-9}	Rb/Cl × 10^{-9}	Mo/Cl × 10^{-9}	Sb/Cl × 10^{-9}	Cs/Cl × 10^{-9}	Pb/Cl × 10^{-9}	U/Cl × 10^{-9}
LS-A1_2002									584					0.75
LS-A1_2003a									637					5.7
LS-A1_2003b									701					7.2
LS-A1_2003c									624					6.3
LS-A1_2008[a]									441					4.2
LS-A1_2015-1[b]	5.5	18	51	54	190	170	22	120	795	63	10	17	0.12	2.0
LS-A1_2015-2[b]	4.5	19	98	360	210	180	36	110	754	47	9.2	17	0.68	1.5
LS-A1_2016-1[b]	6.2	22	51	12	200	170	39	110	782	36	10	15	1.3	1.5
LS-A1_2016-2[b]	10	22	55	83	180	250	30	130	789	59	13	15	1.6	1.6
LS-A1_2016-3[b]	11	31	45	28	170	300	35	140	766	32	10	15	2.1	1.2
LS-A1_2016-4[b]	4.7	18	56	31	200	50	32	170	831	72	12	22	1.7	1.3
LS-A1_2016-5[b]	2.6	20	53	19	180	47	31	150	639	23	6.3	12	1.2	1.0
LS-A1_2016-6[b]	4.3	20	58	150	220	180	35	140	718	31	8.3	16	1.8	1.0
LS-A1_2016-7[b]	3.9	22	49	98	200	150	41	130	819	33	7.8	17	1.0	1.1
LS-A1_2017[b]	1.8	26	44	210	200	36	29	160	741	40	8.7	14	1.8	1.0
LS-A1_2018	2.2	20	58	91	200	33	26	130	731	120	19	12	0.29	1.3
LS-A1_2019	3.5	17	52	100	200	47	37	130	812	33	7.1	12	0.88	1.0
LS-A1_2020	9.1	23	62	150	200	500	28	100	746	39	8.0	13	2.2	1.0
LS-A1_2021	3.1	20	63	270	190	440	22	150	783	49	11	13	2.2	1.1
LS-A2_2008[a]									429					4.4
LS-A3_2015-2	9.9	21	95	4.6	160	290	6.3	170	205	140	2.4	4.0	0.22	2.8
LS-A3_2016-2	2.4	25	69	9.2	300	52	5.1	320	111	190	9.1	2.6	0.23	2.1
LS-A3_2016-3	19	28	87	88	210	490	7.0	190	222	130	6.0	2.8	0.41	5.1
LS-A3_2016-5	3.7	23	73	13	190	42	6.0	160	100	160	3.2	1.6	0.080	5.2
LS-A3_2016-6	4.1	19	85	14	190	110	6.1	190	219	190	2.7	3.7	0.079	3.5
LS-A3_2016-7	3.6	13	83	67	320	80	14	130	575	79	11	6.1	0.40	3.0
LS-A3_2017	2.2	19	77	10	180	85	6.5	250	183	260	5.6	2.3	0.35	4.2
LS-A4_2016-1	3.6	15	150	120	310	100	5.5	130	266	170	6.2	5.3	0.35	6.9
LS-A4_2016-3	7.0	25	72	13	350	250	5.0	170	134	200	16	2.8	1.3	3.7
LS-A4_2016-5	2.7	24	97	13	180	46	6.3	230	94.7	210	6.8	1.0	0.12	4.4
LS-A4_2016-6	7.2	26	93	8.9	190	260	5.7	280	112	190	5.6	1.8	0.13	3.0
LS-A4_2016-7	2.7	25	110	50	480	140	7.2	210	219	270	18	3.3	0.85	2.7
LS-A4_2017	2.6	28	80	10	310	140	7.4	260	142	200	10	3.9	0.83	2.0
LS-A4_2018	1.0	43	93	53	330	65	6.6	180	140	170	13	2.0	0.71	1.8
LS-A4_2019	3.8	27	97	74	370	140	7.1	230	144	180	6.5	1.7	0.43	1.8
LS-A4_2020	2.0	47	99	130	410	770	6.4	330	137	160	8.2	2.6	0.32	1.3
LS-A5_2016-2	8.2	27	95	11	230	120	4.6	210	93.0	190	4.8	1.4	0.21	2.2
LS-A5_2016-3	4.8	25	100	10	310	160	4.7	170	111	210	3.8	2.3	0.11	1.4
LS-A5_2017	5.2	26	93	13	200	360	5.6	160	111	200	8.7	1.3	0.26	2.8
LS-A6_2017	3.5	25	66	11	210	37	6.3	110	320	78	3.4	4.2	0.23	2.3
LS-A6_2018	3.2	21	160	270	340	77	6.2	140	294	110	24	5.3	1.0	11

Table A1. (Continued)

	Al/Cl × 10^{-6}	Ti/Cl × 10^{-9}	Co/Cl × 10^{-9}	Ni/Cl × 10^{-9}	Cu/Cl × 10^{-9}	Zn/Cl × 10^{-9}	Ge/Cl × 10^{-9}	As/Cl × 10^{-9}	Rb/Cl × 10^{-9}	Mo/Cl × 10^{-9}	Sb/Cl × 10^{-9}	Cs/Cl × 10^{-9}	Pb/Cl × 10^{-9}	U/Cl × 10^{-9}
LS-A6_2019	3.0	19	140	190	180	47	7.0	300	155	120	28	1.0	0.21	12
LS-B1_2002									758					2.1
LS-B2_2021	3.1	21	76	140	190	34	10	390	264	160	27	3.4	1.3	2.5
LS-D1_2002									732					6.4
LS-D1_2003									977					2.9
LS-D1_2008 [a]									538					10
LS-D1_2017	2.3	30	52	7.7	230	78	48	140	821	44	10	6.5	1.4	1.5
LS-D1_2018	6.6	24	51	11	190	240	31	180	805	110	23	6.2	0.68	2.5
LS-D1_2019	3.3	22	59	23	190	95	56	150	826	48	10	7.5	0.69	1.5
LS-D1_2020	10	26	65	73	200	740	51	170	915	41	10	10	1.5	0.78
LS-D1_2021	2.3	22	74	140	220	260	65	200	931	75	15	10	1.1	2.0
LS-D2_2008 [a]									790					1.7
LS-D3_2002									558					8.9
LS-E1_2008 [a]									548					2.1
LS-E1_2017	2.3	27	87	69	220	95	110	120	660	40	3.3	13	0.63	0.45
LS-E1_2018	4.3	23	110	440	220	65	98	170	659	100	17	14	2.9	1.0
LS-E1_2019	3.1	28	75	46	200	71	110	130	658	35	2.5	13	0.74	0.32
LS-E1_2020	10	32	120	420	220	600	90	140	703	52	4.5	15	1.8	0.52
LS-E1_2021	2.6	25	67	75	210	89	93	160	684	32	3.0	14	0.87	0.29
LS-E2_2002									617					9.6
LS-E3_2017	3.5	27	80	190	340	88	160	120	604	40	4.0	9.5	1.3	0.35
LS-E4_2021	3.6	25	110	400	210	410	110	140	589	59	7.1	11	2.7	0.91
LS-F1_2002									1020					8.4
LS-F1_2003									904					4.9
LS-F1_2008 [a]									663					0.63
LS-F2_2008 [a]									878					0.79
LS-F3_2008 [a]									832					0.47
Seawater	0.07	38	12	210	26	140	1.5	64	2572	191	5.0	4.1	0.27	25.4
minimum	0.98	12.9	44	5	160	33	4.6	100	93.0	23	2.4	1.0	0.079	0.29
maximum	19	47	160	440	480	770	160	390	1020	270	28	22	2.9	11.6
average	4.8	24	80	99	235	189	33	176	542	109	9.8	8.2	0.92	3.1
SD	3.3	5.9	27	115	71	181	36	63	285	71	6.2	5.8	0.73	2.8

Table A2. Matrix of Pearson's correlation coefficient of all MV LS samples (n = 68), r higher than 0.7 or lower than -0.7 in red color.

	pH	**ORP**	**mud wt**	**Cl^-**	**TA**	**Na**	**Ca**	**Mg**	**B**	**K**	**Br**	**Si**	**Sr**	**S**
Temperature	-0.11	-0.18	0.11	0.37	-0.12	0.43	0.35	-0.27	0.44	0.31	0.33	-0.06	0.27	0.14
pH		-0.21	0.04	-0.21	-0.24	-0.23	-0.32	-0.03	-0.23	0.15	0.14	0.16	0.06	0.45
ORP			-0.44	-0.17	-0.23	-0.10	-0.06	-0.16	0.11	0.13	-0.23	0.17	0.18	0.06
mud wt				0.08	0.11	0.10	0.17	-0.02	-0.10	-0.09	0.14	-0.49	-0.11	-0.08
Cl^-					0.17	0.91	0.86	0.14	0.81	0.25	0.73	0.00	0.21	0.24
TA						0.16	0.14	0.79	-0.10	-0.59	-0.03	0.04	-0.64	-0.28
Na							0.90	0.11	0.88	0.26	0.73	-0.01	0.19	0.35
Ca								-0.12	0.75	0.11	0.76	-0.10	-0.07	0.19
Mg									0.04	0.23	-0.07	-0.06	0.52	0.13
B										0.47	0.51	0.07	0.40	0.43
K											0.09	-0.29	0.86	0.46
Br												0.02	-0.05	0.22
Si													-0.17	-0.26
Sr														0.38
S														
Ba														
Mn														
Fe														
I														
Li														
Al														
Ti														
Co														
Ni														
Cu														
Zn														
Ge														
As														
Rb														
Mo														
Sb														
Cs														
Pb														
U														
δD														
$\delta^{18}O$														
d-excess														
$\Delta^{17}O$														
$^{87}Sr/^{86}Sr$														

Table A2. (Continued)

	Ba	Mn	Fe	I	Li	Al	Ti	Co	Ni	Cu	Zn	Ge	As	Rb
Temperature	0.24	-0.32	-0.12	0.04	0.29	-0.04	-0.18	-0.21	-0.10	0.07	0.00	0.08	-0.04	0.37
pH	0.15	-0.18	-0.19	-0.44	0.05	-0.15	0.30	0.03	0.23	0.09	0.33	0.16	0.25	-0.01
ORP	0.07	-0.24	-0.26	-0.07	0.22	0.28	-0.02	0.05	0.32	0.00	0.24	0.20	-0.06	0.16
mud wt	-0.09	0.12	0.07	0.08	-0.07	-0.14	-0.18	-0.16	-0.23	-0.15	-0.23	-0.24	0.02	-0.07
Cl^-	-0.02	0.08	-0.01	0.09	0.03	-0.13	0.16	0.10	-0.19	0.42	-0.19	-0.24	0.11	0.07
TA	-0.57	0.86	0.38	0.38	-0.86	-0.11	0.13	0.52	-0.33	0.38	-0.19	-0.66	0.46	-0.85
Na	-0.07	0.07	0.11	0.05	0.01	-0.10	0.11	0.11	-0.14	0.41	-0.06	-0.19	0.10	0.06
Ca	-0.23	0.17	0.08	0.21	-0.04	-0.14	0.02	0.03	-0.21	0.35	-0.22	-0.26	0.00	0.03
Mg	0.44	0.23	0.17	-0.12	-0.29	0.12	0.31	0.58	-0.29	0.43	0.00	-0.55	0.58	-0.26
B	0.11	-0.22	-0.03	-0.10	0.31	0.00	0.11	0.00	0.00	0.30	-0.08	0.19	-0.09	0.29
K	0.51	-0.61	-0.30	-0.47	0.72	0.10	-0.02	-0.30	0.41	-0.13	0.00	0.60	-0.39	0.71
Br	-0.18	0.20	0.07	0.20	-0.09	-0.34	0.17	0.11	0.02	0.36	-0.08	-0.08	0.13	-0.05
Si	-0.04	0.01	-0.01	0.12	-0.10	-0.18	0.61	0.15	-0.05	0.43	0.19	0.23	0.30	-0.17
Sr	0.62	-0.49	-0.19	-0.42	0.62	0.19	-0.08	-0.15	0.47	-0.18	0.02	0.79	-0.42	0.57
S	0.02	-0.25	-0.08	-0.43	0.18	0.15	0.12	0.05	0.37	0.03	0.60	0.10	0.14	0.19
Ba		-0.38	-0.13	-0.35	0.43	0.11	-0.05	-0.23	0.19	-0.28	0.20	0.58	0.22	0.42
Mn			0.47	0.54	-0.82	-0.18	0.05	0.66	-0.23	0.34	-0.19	-0.65	0.37	-0.82
Fe				0.20	-0.42	0.05	-0.15	0.22	-0.19	-0.21	0.01	-0.26	0.22	-0.39
I					-0.35	-0.30	-0.24	0.18	-0.23	0.11	-0.56	-0.26	0.08	-0.38
Li						0.13	-0.21	-0.48	0.41	-0.37	0.07	0.73	-0.59	0.94
Al							-0.05	-0.14	-0.06	-0.30	0.51	-0.09	-0.22	0.15
Ti								0.10	-0.07	0.42	0.36	0.01	0.27	-0.25
Co									0.36	0.47	0.02	-0.15	0.24	-0.56
Ni										-0.04	0.22	0.43	-0.19	0.27
Cu											0.05	-0.18	0.28	-0.38
Zn												0.02	0.01	0.09
Ge													-0.43	0.55
As														-0.58
Rb														
Mo														
Sb														
Cs														
Pb														
U														
δD														
$\delta^{18}O$														
d-excess														
$\Delta^{17}O$														
$^{87}Sr/^{86}Sr$														

Table A2. (Continued)

	Mo	**Sb**	**Cs**	**Pb**	**U**	**δD**	**$\delta^{18}O$**	**d-excess**	**$\Delta^{17}O$**	**$^{87}Sr/^{86}Sr$**	**$\delta^{88}Sr$**
Temperature	-0.12	0.08	0.21	0.04	-0.16	-0.24	0.07	-0.21	-0.46	0.28	-0.18
pH	0.03	0.17	-0.11	0.22	-0.17	0.04	-0.12	0.17	-0.04	0.24	-0.27
ORP	-0.18	0.09	0.23	0.23	-0.11	-0.11	-0.07	0.03	0.17	0.15	-0.22
mud wt	0.23	0.00	-0.10	-0.29	0.17	-0.17	-0.14	0.09	0.15	-0.08	-0.02
Cl^-	0.24	0.21	0.03	-0.06	0.12	0.25	0.65	-0.70	-0.37	0.03	-0.01
TA	0.74	0.00	-0.74	-0.62	0.63	0.40	0.18	-0.03	-0.09	-0.61	0.64
Na	0.21	0.05	0.07	-0.07	0.09	0.20	0.65	-0.72	-0.35	-0.01	0.03
Ca	0.12	0.15	0.16	-0.09	0.07	0.17	0.62	-0.70	-0.28	-0.24	0.09
Mg	0.88	-0.02	-0.84	-0.52	0.47	0.32	0.18	-0.07	-0.11	0.55	0.11
B	-0.07	-0.07	0.32	0.14	0.03	0.11	0.62	-0.73	-0.37	0.23	-0.26
K	-0.71	0.30	0.64	0.57	0.26	-0.09	0.06	-0.12	-0.05	0.82	-0.78
Br	0.10	0.33	0.08	0.04	-0.04	0.11	0.40	-0.46	-0.32	-0.22	0.10
Si	0.22	-0.19	-0.17	0.02	-0.62	0.18	0.38	-0.38	-0.15	-0.21	0.16
Sr	-0.68	0.07	0.60	0.58	0.25	-0.08	0.13	-0.21	-0.09	0.97	-0.64
S	-0.21	0.16	0.16	0.33	0.33	0.12	0.23	-0.23	-0.37	0.34	-0.24
Ba	-0.47	0.08	0.25	0.36	0.07	-0.15	-0.07	0.01	0.12	0.68	-0.47
Mn	0.68	0.06	-0.70	-0.54	0.27	0.40	0.14	0.03	0.02	-0.49	0.68
Fe	0.35	-0.08	-0.35	-0.33	0.17	0.08	-0.01	0.05	-0.02	-0.19	0.40
I	0.32	0.10	-0.11	-0.38	-0.18	-0.15	-0.01	-0.06	-0.12	-0.47	0.48
Li	-0.89	0.03	0.85	0.63	-0.24	-0.29	-0.06	-0.07	0.03	0.57	-0.81
Al	-0.14	-0.14	0.11	0.15	0.14	-0.07	-0.09	0.07	0.28	0.22	-0.03
Ti	0.19	-0.08	-0.24	0.01	-0.25	0.25	0.25	-0.19	-0.03	-0.07	-0.02
Co	0.50	0.18	-0.46	-0.21	0.61	0.59	0.32	-0.12	-0.06	-0.27	0.25
Ni	-0.35	0.20	0.36	0.57	0.00	0.05	-0.05	0.09	0.06	0.39	-0.42
Cu	0.40	0.21	-0.33	-0.13	0.14	0.47	0.55	-0.32	-0.02	-0.26	0.17
Zn	-0.11	-0.13	0.04	0.24	-0.23	0.14	0.02	0.04	0.34	0.03	0.02
Ge	-0.61	-0.21	0.51	0.47	-0.49	-0.32	-0.08	-0.06	-0.02	0.72	-0.71
As	0.66	0.33	-0.58	-0.28	0.25	0.21	0.10	0.00	-0.02	-0.41	0.35
Rb	-0.83	0.09	0.86	0.57	-0.19	-0.29	-0.05	-0.08	0.04	0.56	-0.77
Mo		0.12	-0.77	-0.52	0.38	0.37	0.28	-0.17	-0.19	-0.73	0.69
Sb			-0.03	0.19	0.44	0.26	0.10	0.00	-0.03	0.12	-0.25
Cs				0.60	-0.48	-0.39	-0.07	-0.11	0.05	0.50	-0.56
Pb					-0.36	-0.18	0.01	-0.11	0.01	0.44	-0.52
U						0.32	-0.07	0.25	0.09	0.30	-0.07
δD							0.67	-0.35	0.17	-0.09	0.18
$\delta^{18}O$								-0.93	-0.15	-0.14	0.09
d-excess									0.28	0.13	-0.02
$\Delta^{17}O$										0.13	0.01
$^{87}Sr/^{86}Sr$											-0.65